Description of induced nuclear fission with Skyrme energy functionals. II. Finite temperature effects

N. Schunck,[1] D. Duke,[2] and H. Carr[2]
[1]*Physics Division, Lawrence Livermore National Laboratory, Livermore, California 94551, USA*
[2]*School of Computing, University of Leeds, United Kingdom*
(Received 23 January 2015; published 25 March 2015)

Understanding the mechanisms of induced nuclear fission for a broad range of neutron energies could help resolve fundamental science issues, such as the formation of elements in the universe, but could have also a large impact on societal applications in energy production or nuclear waste management. The goal of this paper is to set up the foundations of a microscopic theory to study the static aspects of induced fission as a function of the excitation energy of the incident neutron, from thermal to fast neutrons. To account for the high excitation energy of the compound nucleus, we employ a statistical approach based on finite temperature nuclear density functional theory with Skyrme energy densities, which we benchmark on the ^{239}Pu(n,f) reaction. We compute the evolution of the least-energy fission pathway across multidimensional potential energy surfaces with up to five collective variables as a function of the nuclear temperature and predict the evolution of both the inner and the outer fission barriers as a function of the excitation energy of the compound nucleus. We show that the coupling to the continuum induced by the finite temperature is negligible in the range of neutron energies relevant for many applications of neutron-induced fission. We prove that the concept of quantum localization introduced recently can be extended to $T > 0$, and we apply the method to study the interaction energy and total kinetic energy of fission fragments as a function of the temperature for the most probable fission. While large uncertainties in theoretical modeling remain, we conclude that a finite temperature nuclear density functional may provide a useful framework to obtain accurate predictions of fission fragment properties.

DOI: 10.1103/PhysRevC.91.034327 PACS number(s): 21.60.Jz, 24.75.+i, 25.85.Ec, 27.90.+b

I. INTRODUCTION

One of the most important challenges for a theory of induced fission is the capability to predict the evolution of observables such as the charge, mass, relative yields, total kinetic energy, total excitation energy, and decay patterns of fission fragments as a function of the energy of the incident neutron. Recall that the energy of neutrons produced in induced fission follows roughly a Maxwellian distribution, and the energy range of interest for applications is typically between a few eV and up to about 14 MeV [1,2]. Following an original idea by Bohr and Wheeler, induced fission is modeled as the breakup of the compound nucleus formed by absorption of the incident neutron [3]. In this picture, neutron kinetic energies of the order of the MeV correspond to very high excitation energies of the compound nucleus, where the nuclear level density is very large [4].

In a density functional theory (DFT) approach to induced fission, one may be tempted to describe such highly excited states directly, via various general schemes such as the random phase approximation or the generator coordinate method. However, even assuming all of these methods were properly defined for the kind of energy densities used in practice (cf. the discussions about multireference DFT in Refs. [5–9]), the very large density of states to consider may jeopardize the success of such a strategy. In addition, it is expected that dissipation plays a role in fission, and extensions of these methods to account for explicit couplings between collective and intrinsic degrees of freedom have only recently been outlined [10].

In this context, the finite temperature formulation of the nuclear DFT provides an appealing alternative [11–14]. Assuming that the system is described by a mixed quantum state uniquely determined by the form of the statistical density operator provides a convenient basis to quantify the impact of excitation energy on the deformation properties of the compound nucleus.

There have been many applications of the finite temperature formalism in nuclear structure, including early studies of fission barriers using the Thomas-Fermi approximation [15–20], the Hartree-Fock (FT-HF) approximation [21,22], and more recently at the Hartree-Fock-Bogoliubov (FT-HFB) approximation [23–25], or applications in the calculation of giant dipole resonances and level densities [26–29]. Until now, however, there has been no systematic study of the validity and applicability of finite temperature DFT in the description of induced fission. Of particular importance are the evolution of scission configurations and of fission fragment properties as a function of the excitation energy of the compound nucleus.

In a previous paper, hereafter referred to as (I), we have used the nuclear DFT with Skyrme energy densities to analyze static properties of the neutron-induced fission of the ^{239}Pu nucleus [30]. In particular, we have discussed the role of triaxiality at scission, the dependence on the parametrization of the energy density functional (EDF) (including the pairing channel), and the critical importance of scission configurations. The topological method that we have proposed to identify the latter makes it possible to define a region in the collective space where scission should take place. We have then shown that localization techniques borrowed from electronic structure theory can allow us to approach the asymptotic conditions of two independent fission fragments. This is key to extracting theoretically sound estimates of the total excitation energy of the fragments.

 ©2015 American Physical Society

Building on this previous study, the goals of this second paper are, therefore, (i) to establish and validate the framework for nuclear DFT calculations at finite temperature in the specific context of induced fission, (ii) to study the evolution of fission barriers and the position and nature of scission configurations as functions of the excitation energy of the incident neutron, and (iii) to explore the consequences of the finite temperature description for the determination of fission fragment properties. This paper is the second in a series of several articles focusing on the microscopic description of induced fission within the framework of the nuclear DFT with Skyrme energy densities.

Section II contains a brief reminder of the theoretical framework, from basic definitions and concepts related to neutron-induced nuclear fission to the extension of nuclear DFT at finite temperature with Skyrme functionals. Section III A focuses on the evolution of potential energy surfaces and fission barriers with temperature. Section IV is devoted to fission fragment properties at finite temperature, including the extension of the concept of quantum localization, a study of the coupling to the continuum, and an estimate of the nuclear and Coulomb interaction energy of the fission fragments.

II. THEORETICAL FRAMEWORK

Our theoretical approach is based on the local density approximation of the EDF theory of nuclear structure. We recall in the next few sections some of the basic ingredients of the EDF theory pertaining to the description of induced nuclear fission at given excitation energy.

A. Thermodynamical and statistical view of neutron-induced fission

We begin by recalling a few well-known facts about neutron-induced fission to avoid confusions about the vocabulary used in this work. For fissile elements such as ^{239}Pu, the capture of a thermal neutron (in equilibrium with the environment and with an average kinetic energy of the order of $E_n \approx 0.02$ eV) is sufficient to induce fission. The energy balance of the reaction is such that the compound nucleus (Z,N) formed after the neutron has been captured is at an excitation energy equal to $|S(N)|$, where $S(N)$ is the one-neutron separation energy. In fissile elements, this quantity is larger than the fission barrier height, leading to fission. Note that the concept of nuclear deformation, hence of potential energy surfaces (PESs) and fission barriers, is highly model dependent: It is rooted in the mean-field approach to nuclear structure and originates from the spontaneous symmetry breaking of rotational invariance in the intrinsic frame of the nucleus [31,32]. However, the success of macroscopic-microscopic and self-consistent approaches in describing both qualitatively and quantitatively the main features of the fission process is evidence that such a concept is very useful in practice.

1. Statistical description of the compound nucleus

In a microscopic theory of fission based on nuclear DFT, it is assumed that the fission process is driven by a small set of collective degrees of freedom $\boldsymbol{q}$. It is further assumed that the PES of the compound nucleus in this collective space can be reliably described at the Hartree-Fock-Bogoliubov (HFB) approximation. This implies that the collective variables are defined as expectation values of specific operators, such as, e.g., multipole moments, on the HFB vacuum. The PES is then generated by performing a series of constrained HFB calculations. Such an approach is clearly an approximation, because the HFB vacuum is the lowest energy state for the set of constraints $\boldsymbol{q}$ while the compound nucleus is, by definition, in an excited state. Nonetheless, early calculations of fission fragment charge mass yields and total kinetic energy for low-energy, neutron-induced fission obtained within this approximation give a reasonably good agreement with experimental data [33–35]. In fact, a similar approximation is implicitly made in macroscopic-microscopic methods, with a similarly good reproduction of experimental data [36,37].

If the energy of the incident neutron E_n increases (fast neutrons), the excitation energy E^* of the compound nucleus increases accordingly. For $E_n \approx 14$ MeV, E^* can be typically of the order of 20 MeV or more in actinides. In this regime, the nuclear level density is very large, of the order of $\rho(E^*) \approx 10^{12}$ MeV^{-1} at $E^* \approx 20$ MeV, and growing exponentially with E^*; see, e.g., Ref. [26]. It thus becomes more and more unlikely that constrained HFB vacua can still provide a realistic description of the nuclear PES and more generally of the fission process. In addition, the extremely large level density suggests that direct calculation of excited states could prove extremely challenging. Instead, we seek to describe induced fission with finite temperature density functional theory (FT-DFT).

In this work, we neglect particle evaporation or γ emission. In other words, we do not consider second chance fission—the fission of the nucleus after one neutron has been emitted—or third chance fission—after two neutrons have been emitted. Therefore, the compound nucleus is viewed as a closed and isolated system. In statistical physics, such systems should be treated in the microcanonical ensemble [38]. However, counting the number $\mathcal{N}(E^*)$ of microstates of the system at any given experimental excitation energy E^* would require one to have access to the full eigenspectrum of the nucleus. In practice, this is impossible and the microcanonical treatment of the problem must be ruled out [29].

In nuclear DFT, the nuclear wave function takes the form of a HFB vacuum: It is not an eigenfunction of the nuclear Hamiltonian or of the particle number operator. This implies that the total energy and the number of particles in the system are only known on average: There can be fluctuations of both quantities, of either quantum or/and statistical origin [29]. This observation suggests to use the grand-canonical ensemble to describe the nuclear system. The density operator $\hat{D}$ characterizing such an ensemble is obtained by maximizing Gibbs entropy under the constraints that the energy and particle numbers are constant on average. The resulting equation is equivalent to expressing the thermodynamical grand potential Ω at constant temperature T and chemical potential λ in terms of the grand partition function. The relevant thermodynamic potential is then the Helmholtz free energy F [38]. Note that, in this statistical setting, the temperature T is, *stricto sensu*, only

a Lagrange parameter used to maintain the energy constant on average.

2. *Neutron incident energy and nuclear temperature*

One of the difficulties in the FT-DFT description of fission is to interpret the temperature introduced in the theory, in particular in terms of the excitation energy of the compound nucleus. It was suggested in Refs. [39,40] that the temperature T be determined locally at every point in the collective space by assuming that all the excitation energy at deformation $\boldsymbol{q}$ is entirely of thermal nature. In practice, this scenario has only been applied in the macroscopic-microscopic approach to nuclear structure. Starting from the total energy at $T = 0$, expressed as the sum of a macroscopic term, a shell correction, and a pairing correction, one determines the local temperature $T(\boldsymbol{q})$ given the experimental excitation energy E^*; this temperature is then used to generate a new, temperature-dependent PES where shell and pairing corrections are locally damped. This procedure has been used to describe superdeformed bands at high spin and high excitation energy [41], hyperdeformation and the Jacobi shape transition [42], and the dynamics of induced fission [43].

The feasibility of such an approach, however, is entirely contingent on the assumed decomposition of the energy into a temperature-independent part (the liquid drop energy) and a temperature-dependent microscopic correction, both of which depend on deformation. In FT-DFT, such a decomposition does not exist. All of the total energy is a function of the temperature: If one followed the recipe of selecting at point $\boldsymbol{q}$ in the collective space the DFT solution at $T = T(\boldsymbol{q})$ such that $E(\boldsymbol{q}) = E^*$, the total energy of the nucleus would become, by construction, constant across the collective space, and the very concept of a PES with barriers and valleys would be lost.

To retain the view of fission as a large amplitude collective motion through a PES while simultaneously accounting for the effect of excitation energy via FT-DFT, we are thus bound to make the additional assumption that the temperature must be constant across the PES. More specifically, the PES can be defined either as the function $F(\boldsymbol{q}; T)$, where F is the Helmholtz free energy, or by the function $E(\boldsymbol{q}; S)$, where S is the entropy; see Sec. III A for additional details. In addition, because fission occurs for all neutron energies of interest, we assume that the total excitation energy E^* of the compound nucleus must be higher than the top of the barrier computed at $S > 0$: This requirement gives us the maximum allowable *thermal* excitation energy U available to the system. Figure 1 illustrates how this works in practice: The thermal excitation energy is related to the entropy S of the FT-HFB theory through $E_n + S(N) = U(S) + E_{\rm A}$, where E_n is the kinetic energy of the incident neutron, $S(N)$ is the one-neutron separation energy of the compound nucleus, and $E_{\rm A}$ is the height of the first fission barrier at $S = 0$. In calculations with energy functionals, the height of the first fission barrier may be larger than the separation energy, $E_A > S(N)$, which would contradict the experimental observation that the nucleus is fissile. For example, for ^{240}Pu, we find $S(N) = 7.09$ MeV and $E_{\rm A} = 7.65$ MeV. To guarantee that thermal neutrons trigger fission, we thus have to introduce a small offset

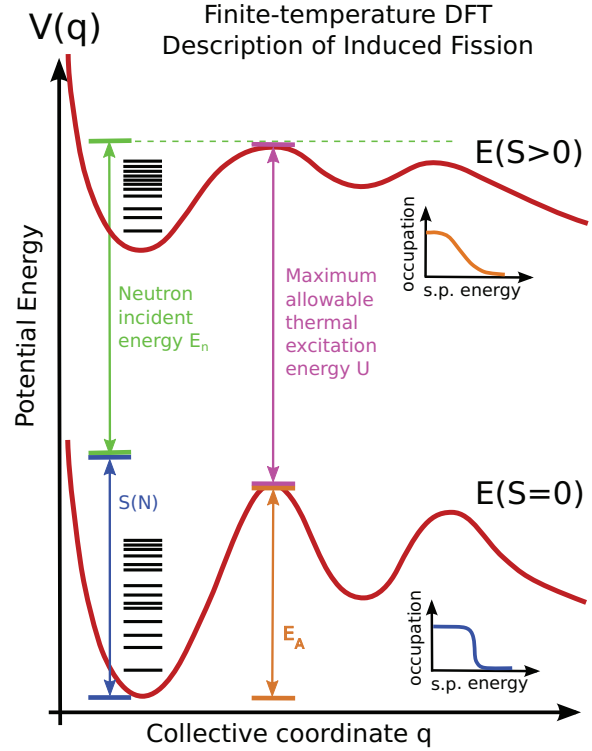

FIG. 1. (Color online) Schematic illustration of how induced fission is described within DFT at finite temperature. The separation energy of the compound nucleus (Z,N) is denoted $S(N)$.

$\delta = E_{\rm A} - S(N)$ such that $E_n + S(N) + \delta = U(S) + E_{\rm A}$. In this particular case, $U(S) = E_n$. Note that this offset is a purely empirical correction needed to guarantee the fissile nature of the compound nucleus.

To finish this section, we note that the most rigorous way to combine a statistical description of the compound nucleus at high excitation energy with the conventional view of fission as a large-amplitude collective motion would be to use the Liouville equation for the grand-canonical density operator. Starting from some initial condition $\hat{D}_0$, the Liouville equation gives the time evolution of $\hat{D}$. A collective, time-dependent equation of motion for the nucleus could then be obtained, at least in principle, by introducing the HFB approximation for the density operator and a small set of collective variables that would carry the time dependence. Such a procedure was outlined in a recent paper, but numerous challenges remain to implement it in practice [44].

B. Finite temperature HFB theory

As recalled above, we use the finite temperature HFB theory to describe the compound nucleus at given excitation energy. The FT-HFB theory has a long history in the literature [13,14,27,28,45–48]. Here we only recall the physical assumptions that are most relevant to this work. The compound nucleus is assumed to be in a state of thermal equilibrium at temperature T. In the grand-canonical ensemble, the system

is then characterized by the statistical density operator $\hat{D}$,

$$\hat{D} = \frac{1}{Z} e^{-\beta(\hat{H}-\lambda\hat{N})}, \tag{1}$$

where Z is the grand partition function, $\beta = 1/kT$, $\hat{H}$ is the Hamiltonian of the system, λ the Fermi level, and $\hat{N}$ the number operator [13,38]. In this work, the Hamiltonian is a two-body effective Hamiltonian with the Skyrme pseudopotential. The statistical average $\langle\hat{F}\rangle$ of an operator $\hat{F}$ is defined as

$$\langle\hat{F}\rangle = \mathrm{Tr}[\hat{D}\hat{F}], \tag{2}$$

where the trace can be computed in any convenient basis of the Fock space; i.e., it involves many-body states.

In the mean-field approximation of the density operator, the real Hamiltonian $\hat{H}$ is replaced with a quadratic form $\hat{K}$ of the particle operators [13,27,28,48]. Given a generic basis $|i\rangle$ of the single-particle space, with c_i and $c_i^\dagger$ the corresponding single-particle operators, this is expressed by

$$\hat{K} = \sum_{ij} K_{ij} c_i^\dagger c_j \ \text{(HF)}, \tag{3}$$

$$\hat{K} = \frac{1}{2}\sum_{ij} K_{ij}^{11} c_i^\dagger c_j + \frac{1}{2}\sum_{ij} K_{ij}^{22} c_i c_j^\dagger + \frac{1}{2}\sum_{ij} K_{ij}^{20} c_i^\dagger c_j^\dagger + \frac{1}{2}\sum_{ij} K_{ij}^{02} c_i c_j \ \text{(HFB)}, \tag{4}$$

where HF refers to the Hartree-Fock approximation of the partition function, and HFB refers to the HFB approximation. As a consequence of the Wick theorem for ensemble averages, there is a one-to-one correspondence between the one-body density matrix $\hat{\rho}$ (HF) or generalized density matrix $\hat{\mathcal{R}}$ (HFB) and the operator $\hat{K}$ [13,28]. In particular, all statistical traces can be computed by taking the trace in the single-particle space [13],

$$\langle\hat{F}\rangle = \mathrm{Tr}[\hat{D}\hat{F}] = \begin{cases} \mathrm{tr}\left[\hat{\rho}\hat{F}\right], \ \text{(HF)}, \\ \frac{1}{2}\mathrm{tr}[\hat{\mathcal{R}}\hat{F}], \ \text{(HFB)}. \end{cases} \tag{5}$$

The forms (3) and (4) of the operator $\hat{K}$ defining the statistical density operator are generic. The matrix elements of $\hat{K}$ are thus taken as variational parameters and determined by requesting that the grand potential be minimum with respect to variations $\delta\hat{K}$. This leads to the identification $\hat{K} = \hat{h}$ (HF) and $\hat{K} = \hat{\mathcal{H}}$ (HFB); that is,

$$\hat{\rho} = \frac{1}{1+\exp(\beta\hat{h})}, \ \text{(HF)}, \tag{6}$$

$$\hat{\mathcal{R}} = \frac{1}{1+\exp(\beta\hat{\mathcal{H}})}, \ \text{(HFB)}, \tag{7}$$

where $\hat{h}$ is the usual HF Hamiltonian, $\hat{\mathcal{H}}$ the HFB Hamiltonian, and $\beta = 1/kT$. These equations are the HF and HFB equations; see Refs. [13,28] for the demonstration. Note that the variational principle does not require that either of these matrices be diagonalized. In practice, building the density matrix (generalized density) from the eigenvectors of h ($\mathcal{R}$) just happens to be a very convenient way to guarantee that the functional equations (6) and (7) are satisfied.

In the basis where $\mathcal{H}$ is diagonal, one easily shows that the statistical occupation of a one quasiparticle (qp) state reads

$$\mathrm{Tr}[\hat{D}\beta_\mu^\dagger\beta_\mu] = \frac{1}{1+e^{\beta E_\mu}}\delta_{\mu\nu} = f_{\mu\nu}\delta_{\mu\nu}, \tag{8}$$

with E_μ the qp energy, i.e., the eigenvalue of $\mathcal{H}$. This result allows to show that the matrix of the one-body density matrix and pairing tensor in the single-particle (sp) basis are modified according to

$$\rho_{ij} = \mathrm{Tr}[\hat{D}c_j^\dagger c_i] = [V^*(1-f)V^T]_{ij} + (UfU^\dagger)_{ij}, \tag{9}$$

$$\kappa_{ij} = \mathrm{Tr}[\hat{D}c_j c_i] = [V^*(1-f)U^T]_{ij} + (UfV^\dagger)_{ij}, \tag{10}$$

where the U and V are the matrices of the Bogoliubov transformation.

The finite temperature extension of the HFB theory poses two difficulties. First, we recall that, in the HFB theory at zero temperature, the component V_μ of the qp μ is always localized for a system with negative Fermi energy $\lambda < 0$ [49,50]. The consequence is that the mean-field, the pairing field, and the expectation value of any physical observable $\hat{O}$ are also localized (because $\rho = V^*V^T$ and $O = \mathrm{tr}\hat{O}\hat{\rho}$). However, at finite temperature, we note that, even though the pairing tensor remains always localized for $\lambda < 0$, the density matrix does not. More specifically, all qps μ with $0 < E_\mu < -\lambda$ give a localized contribution to the mean-field and physical observables, while all qps with $E_\mu > -\lambda$ yield a coupling with the continuum through the $\left(UfU^\dagger\right)$ term of the density matrix; see Sec. IV D for more details. The existence of this coupling was already pointed out and quantified in the context of the Hartree-Fock theory at finite temperature [22,51,52].

The second difficulty is that, in the statistical description of the system by a grand-canonical ensemble, only the average value of the energy and the particle number (and any other constrained observables) are fixed. In addition to the quantum fluctuations brought about by the fact that DFT wave functions are not eigenstates of the Hamiltonian, thermal (or statistical) fluctuations are also present [29]. They increase with temperature and should decrease with the system size [38]. From a statistical point of view, the FT-HFB theory only gives the most probable solution within the grand-canonical ensemble, the one that corresponds to the lowest free energy. Mean values and deviations around the mean values of any observable $\hat{\mathcal{O}}$ can be computed in the classical limit as in Ref. [48],

$$\bar{\mathcal{O}} = \frac{\int d^N\boldsymbol{q}\ \mathcal{O}(\boldsymbol{q})e^{-\beta F(T,\boldsymbol{q})}}{\int d^N\boldsymbol{q}\ e^{-\beta F(T,\boldsymbol{q})}}. \tag{11}$$

Such integrals should, in principle, be computed across the whole collective space defined by the variables $\boldsymbol{q} = (q_1,\ldots,q_N)$ and require the knowledge of the volume element $d^N\boldsymbol{q}$. Other possibilities involve functional integral methods [53]. In this work, we only consider the most probable value for observables and disregard all statistical fluctuations.

C. Skyrme EDF and numerical and numerical implementation

We briefly recall that we work with Skyrme energy densities, for which the energy of the nucleus is a functional of the one-body density matrix. In this paper, all calculations have been performed at the FT-HFB level with the SkM* parametrization of the Skyrme pseudopotential [54]. The pairing functional originates from a density-dependent, mixed surface-volume pairing force. In the calculations of the densities, all quasiparticles above a cutoff energy $E_{\rm cut} = 60$ MeV are dismissed. The pairing strength for both the proton and the neutron forces were fitted locally on the three-point formula of the odd-even mass difference in ^{240}Pu; see (I) for details. Contrary to (I), the UNEDF family of functionals was not considered here, because they require the Lipkin-Nogami prescription, which is not available yet at finite temperature.

As in (I), the nuclear shape is characterized by a set $\boldsymbol{q} = (q_1, \ldots, q_N)$ of N collective variables. In this work, we consider the expectation value $q_{\lambda\mu}$ of the multipole moment operators $\hat{Q}_{\lambda\mu}$ on the HFB vacuum for the axial quadrupole $(\lambda,\mu) = (2,0)$, triaxial quadrupole $(\lambda,\mu) = (2,2)$, axial octupole $(\lambda,\mu) = (3,0)$ and axial hexadecapole $(\lambda,\mu) = (4,0)$. We also employ the expectation value of the neck operator $\hat{Q}_N$ with the range $a_N = 1.0$ fm. The finite-temperature extension of the Wick theorem guarantees that the expectation value of these (one-body) operators at $T > 0$ take the same form as at $T = 0$, only with the density matrix computed as in (9). Constrained HFB solutions are obtained by using a variant of the linear constraint method where the Lagrange parameter is updated based on the cranking approximation of the random phase approximation (RPA) matrix [55–57]. This method has been extended to handle nonzero temperatures. All calculations were performed with the DFT solvers HFODD [57] and HFBTHO [58]. In both codes, the HFB eigenfunctions are expanded on a one-center harmonic oscillator (HO) basis. In all calculations reported here, this expansion was based on the lowest $N_{\rm states} = 1100$ states of the deformed HO basis. The largest oscillator shell entering the expansion was $N_{\rm max} = 31$. The deformation β_2 and the oscillator frequency ω_0 of the HO were parametrized empirically as a function of the requested expectation value q_{20} of the quadrupole moment $\hat{Q}_{20}$ according to

$$\omega_0 = \begin{cases} 0.1 \times q_{20} e^{-0.02 q_{20}} + 6.5 \text{ MeV} & \text{if } |q_{20}| \leqslant 30 \text{ b} \\ 8.14 \text{ MeV} & \text{if } |q_{20}| > 30 \text{ b} \end{cases} \tag{12}$$

and

$$\beta = 0.05\sqrt{q_{20}}. \tag{13}$$

We refer the reader to (I) and Ref. [59] for further details on the convergence properties of the basis.

III. EVOLUTION OF DEFORMATION PROPERTIES AT FINITE TEMPERATURE

In this section, we illustrate the modifications of the collective PESs discussed in (I) induced by the finite temperature. In particular, we give an accurate estimate of the evolution of fission barrier heights as a function of the excitation energy of the compound nucleus formed in the reaction ^{239}Pu(n,f).

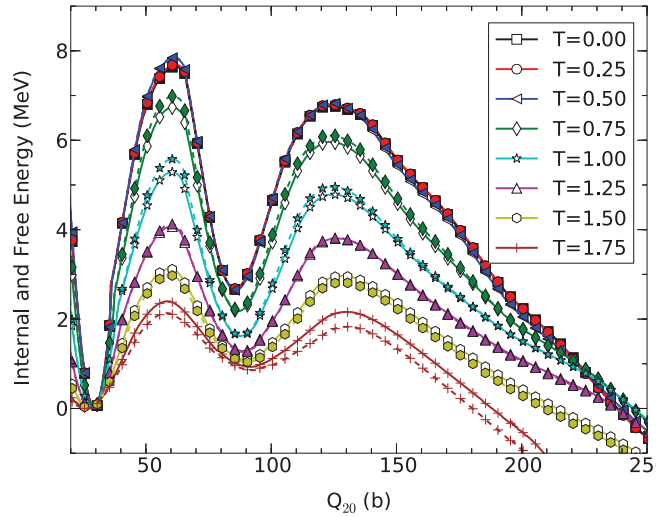

FIG. 2. (Color online) Solid lines with open symbols, free energy along the least-energy fission pathway in ^{240}Pu for finite temperatures $T = 0.00, \ldots, 1.75$ MeV. Dashed lines with solid symbols, corresponding internal energy E at constant entropy S. All curves are normalized to their ground-state values. Temperature units are in MeV.

A. Fission pathway of least energy

As recalled in Sec. II B, the FT-HFB theory is built on the grand-canonical description of the nucleus as a system in thermal equilibrium maintained at constant temperature T. Because particle number is constant, on average, across the whole collective space, the thermodynamical potential relevant to study deformation effects is the Helmholtz free energy $F = E - TS$, which is computed at constant volume V and temperature T. The PES is characterized by the ensemble of points $F(\boldsymbol{q})$, and variations of free energy between two points $\boldsymbol{q}_1$ and $\boldsymbol{q}_2$ are computed through $\delta F|_T = F(\boldsymbol{q}_1, T) - F(\boldsymbol{q}_2, T)$.

We show in Fig. 2 the free energy of the compound nucleus ^{240}Pu along the least-energy fission pathway for temperatures ranging between 0 and 1.75 MeV by steps of 250 keV. Based on the discussion of Sec. II A, this corresponds to maximal excitation energies of about $E^* \approx 80$ MeV for the compound nucleus. Recall that the height of the first fission barrier is $E_{\rm A} = 7.65$ MeV in ^{240}Pu for the SkM* functional; this corresponds to maximum neutron kinetic energies of about $E_n \approx 73$ MeV. The least-energy fission pathway is found according to the procedure presented in (I): While the value of the axial quadrupole moment is constrained, the triaxial, octupole, and hexadecapole moments are unconstrained, so that triaxiality and mass asymmetry effects are taken into account.

It has been argued in the literature that an isentropic description of fission should be preferred over the isothermal description [20,25]. In this representation, the thermodynamical potential is the internal energy E, which is computed at constant volume V and entropy S. The PES is now the ensemble of points $E(\boldsymbol{q})$, and variations of energy are computed through $\delta E|_S = E(\boldsymbol{q}_1; S) - E(\boldsymbol{q}_2; S)$. The Maxwell relations of thermodynamics state that the variations of the free energy $\delta F|_T$ over some extensive state variable X (at constant

temperature) are equal to the variations of the internal energy $\delta E|_S$ (at constant entropy) [38].

Figure 2 also shows the internal energy $E(\boldsymbol{q};S)$ at constant entropy deduced from the free energy curves: At each value $\boldsymbol{q}$ of the constrained collective variable (here the axial quadrupole moment $\hat{Q}_{20}$), the quantities $E(\boldsymbol{q};T)$ and $S(\boldsymbol{q};T)$ are used to reconstruct the relation $E(\boldsymbol{q};S)$ by regression. For each temperature T, the curves $E(\boldsymbol{q};S)$ are then generated by fixing the entropy at its value at the top of the second barrier for that temperature T. Note that we could choose the entropy at other deformations: When properly normalized, the Maxwell relations guarantee that all these choices should be strictly equivalent, within the numerical accuracy of the regression. Figure 2 indicates that this accuracy is of the order of 500 keV, at worst. This confirms earlier calculations [25,60].

The isentropic representation of the fission process is often thought of as more physically justified than the isothermal one, as it has its origin in the separation of scales between the slow collective motion and fast intrinsic excitations of the nucleus [44,61]. This separation justifies the thermodynamical assumption of adiabaticity [62]: Going from point $\boldsymbol{q}$ to point $\boldsymbol{q}'$ in the collective space can be accomplished via a quasistatic, reversible transformation that conserves entropy. By contrast, it is sometimes argued that the absence of a heat bath to maintain the temperature constant invalidates the isothermal representation [20].

Such a statement, however, comes from a misconception about the nature of the heat bath. Indeed, another way to interpret the separation of scales between collective and intrinsic motion is to write the energy density of the fissioning nucleus as

$$\mathcal{H} = \mathcal{H}_{\text{coll}}(\boldsymbol{q}) + \mathcal{H}_{\text{int}}, \tag{14}$$

with the collective part depending only on the collective coordinates $\boldsymbol{q}$ while the intrinsic part depends on all intrinsic degrees of freedom. In a DFT picture, for example, we would take $\mathcal{H}_{\text{int}} = \mathcal{H}_{\text{int}}[\rho,\kappa]$. The number of intrinsic degrees of freedom is given by the value of ρ and κ at every point in space, spin, and isospin space: It is considerably higher than the number of collective variables. In addition, in the limit of no dissipation, the couplings between the two types of motion can be neglected [44]. The decomposition (14), together with the different relaxation scales, shows that the role of the heat bath is, in fact, played by the intrinsic Hamiltonian. In the theory of quantum dissipation, the latter is often modeled by a collection of HOs [63,64]. Passing from point $\boldsymbol{q}$ to point $\boldsymbol{q}'$ can thus also be accomplished through an isothermal process, during which heat will be exchanged between the collective wave packet and the intrinsic excitations, according to $\delta Q = T\,dS$. In our opinion, the two representations, which are mathematically equivalent thanks to the Maxwell equations, are also physically equivalent because they only rely on the hypothesis of the separation of degrees of freedom into slow collective and fast intrinsic motion.

To conclude this section, we note that, for the Maxwell relations to be valid, the respective thermodynamical potentials $F(\boldsymbol{q})|_T$ and $E(\boldsymbol{q})|_S$ must be differentiable at point $\boldsymbol{q}$. As discussed in Sec. IV E, this may not be true near scission, at least in the four-dimensional collective space explored in Fig. 2.

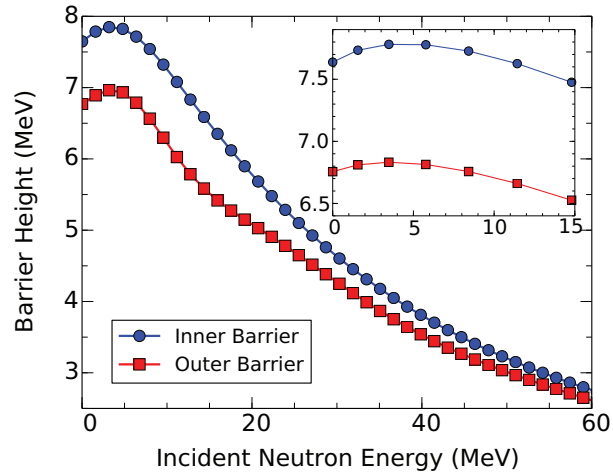

FIG. 3. (Color online) Evolution of the inner and outer barrier heights in ^{240}Pu as a function of the energy of the incident neutron. The inset represents a close-up in the 0–15-MeV region.

B. Dependence of fission barriers on excitation energy

Fission barrier heights (both inner and outer barriers) are particularly important quantities in fission models, as they are often used as input to reaction codes. In Fig. 3, we show the variation of the inner and outer fission barrier heights in ^{240}Pu as a function of the incident neutron energy E_n. As outlined in Sec. II A, we compute the fission barrier at incident neutron energy E_n for the entropy S such that $E_n = U(S)$. The maximum allowable thermal excitation energy is deduced from the $E(\boldsymbol{q})|_S$ curves, which are obtained by spline interpolation over the $F(\boldsymbol{q})|_T$ calculations. Note that at any point $\boldsymbol{q}$, the error on the total energy at given entropy owing to the interpolation is smaller than 50 keV.

In the literature, fission barriers at finite temperature were computed within the macroscopic-microscopic approach [65–68], the semiclassical Thomas-Fermi framework [15–20], and the self-consistent HF theory [19,21]. There are also a few applications of the finite temperature HFB theory with both zero-range Skyrme functionals and finite-range Gogny forces [24,25,69]. All these studies point to the disappearance of the barriers with the excitation energy of the compound nucleus or, equivalently, the nuclear temperature. Our results confirm this overall trend.

However, we emphasize here that this phenomenon occurs at temperatures that are relatively high as far as applications of neutron-induced fission are concerned. In the regime $0 \leqslant E_n < 5$–6 MeV, the somewhat unexpected effect of nuclear temperature is to slightly *increase* fission barriers. In the inset of Fig. 3, we show a close-up of the fission barrier heights in the region $0 \leqslant E_n < 15$ MeV. There is a very clear upward trend at low neutron energies. Although the increase of the fission barriers does not exceed 200 keV, the effect may be significant enough to affect fission fragment distributions.

The reason for the counterintuitive behavior of the barriers may be attributed to the different damping speeds of pairing correlations and shell effects with temperature. In Fig. 4, we show the pairing energy as a function of the FT-HFB temperature for the ground- state, fission isomer, top of

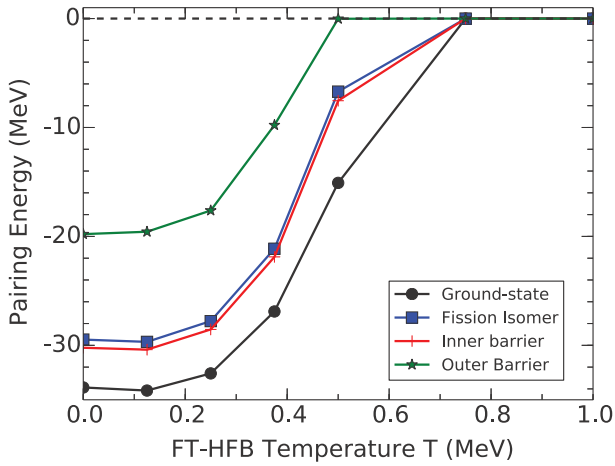

FIG. 4. (Color online) Evolution of pairing energy in the ground-state and fission isomer and at the top of the first barrier and the top of the second barrier in ^{240}Pu as a function of the FT-HFB nuclear temperature.

the first barrier, and top of the second barrier in ^{240}Pu. We find that pairing correlations have vanished completely beyond $T = 0.75$ MeV, which corresponds to a neutron energy of approximately 12 MeV. However, shell effects are still substantial at this temperature [22]. Our interpretation is that the fast damping of pairing correlations attenuates, delays, or even partially reverts the impact of the damping of shell effects on the deformation energy as a function of temperature. Indeed, one of the side-effects of pairing correlations is to reduce deformation energy [40,70], i.e., the energy difference $E_{\rm def}(\boldsymbol{q}) = E(\boldsymbol{q}) - E(\boldsymbol{q} = 0)$. If pairing correlations rapidly decrease as a function of T, the absolute value of the deformation energy may slightly increase as a result. Of course, this qualitative interpretation should be validated by rigorous macroscopic-microscopic calculations.

IV. FISSION FRAGMENT PROPERTIES AT FINITE TEMPERATURE

In (I), we discussed the fission fragment properties of ^{239}Pu(n,f) at $T = 0$ using the joint contour net (JCN) to define a scission region in terms of topological changes of the density, based on the assumption that the variations of the density in the prefragments must be commensurate with those of the density in the compound nucleus. Within this region of scission configurations, we then apply a quantum localization method to disentangle the prefragments to approach the asymptotic conditions of two fully independent fragments. In this section, we extend this study to finite temperature.

A. Definition of a scission region

The fission pathway of lowest free energy across the four-dimensional collective space shown in Fig. 2 was extended up to the scission region for each temperature. We find that the value $q_{20}^{(\rm disc)}$ of the axial quadrupole moment where the first discontinuity in the $F(q_{20})$ curve appears changes with temperature. Table I lists these values as a function of the

TABLE I. Position of the first discontinuity of the $F(q_{20})$ curve along the most probable fission pathway as a function of temperature.

T (MeV)	$q_{20}^{(\rm disc)}(b)$	T (MeV)	$q_{20}^{(\rm disc)}(b)$
0.00	345.0	1.00	332.5
0.25	357.0	1.25	331.0
0.50	339.5	1.50	333.0
0.75	332.0	1.75	333.0

temperature for the SkM* functional. Note that there is a numerical uncertainty of about 2–3 b for the values of q_{20} reported in the table, because calculations converge very slowly near scission. The scission region covers a relatively broad range of $\hat{Q}_{20}$ values of approximately 25 b. Note the original increase of the quadrupole moment at low temperatures: This is caused by the quenching of pairing correlations, which was shown to shift the discontinuity at larger values of $\hat{Q}_{20}$ in (I). Because the discontinuity does not occur at the same q_{20} for all temperatures, the equivalence between the $E(q_{20})|_S$ and $F(q_{20})|_T$ representations of the fission pathway does not hold in the scission region because neither the internal energy nor the free energy are continuous functions over the entire range of quadrupole moments involved.

Following the approach at zero temperature outlined in (I), we introduce an additional constraint on the number of particles in the neck, $\hat{Q}_N$, to explore scission configurations. At each temperature T, the expectation value of $\hat{Q}_N$ is varied in the range $q_N \in [0.1,4.5]$, while the quadrupole moment is fixed at the values listed in Table I. The JCN analysis is then applied at each temperature to the set of neutron and proton densities along these trajectories to identify putative scission configurations. As an illustration, Fig. 5 shows the JCN at $q_N = 0.2$ at both $T = 0.0$ MeV (top) and $T = 1.5$ MeV (bottom).

We recall that the JCN algorithm provides a computational tool for extracting the topological features of a multifield data set, which includes connectivity between regions of different behaviors. It was first introduced in the context of nuclear structure in Ref. [71] and applied in (I) to the specific problem of defining scission configurations along a continuous fission pathway for neutron-induced fission. The JCN analysis involves generalizing one-dimensional scalar analysis to capture simultaneous variation in multiple output functions of the type $(f_1,\ldots,f_n) : \mathbb{R}^3 \to \mathbb{R}^n$. In (I), we concluded that the JCN could be a useful tool to define plausible scission configurations. In particular, the appearance of a branching structure in the JCN, which characterizes the existence of two distinct regions in space, was interpreted as the precursor to scission; the subsequent development of "starbursts" in each branch was associated with the completion of scission, as these starbursts indicate that the variations of the density in each fragment is commensurate to those of the density in the whole nucleus (hence, suggesting two well-defined fragments). We also observed that this identification is independent of the numerical parameters used in the JCN.

The results of the JCN analysis for the least-energy fission pathway of ^{240}Pu at finite temperature are summarized in Table II. As in (I), we define an interval $I_q = [q^{(\rm min)},q^{(\rm max)}]$

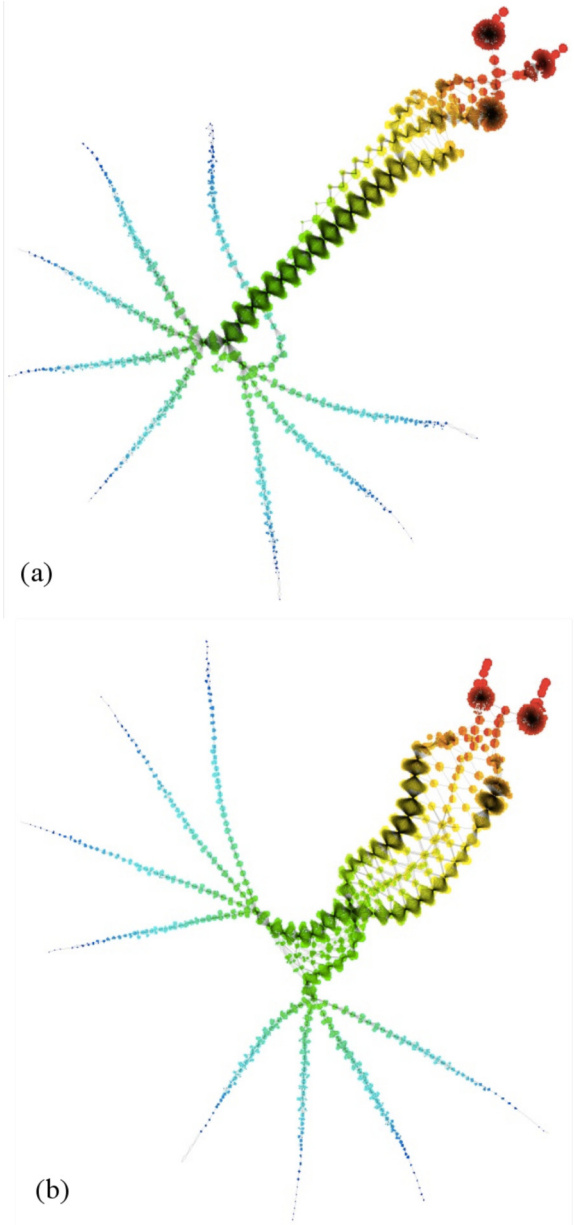

FIG. 5. (Color online) Joint contour net graph of the densities at $q_N = 0.2$ at temperature $T = 0.00$ MeV (a) and $T = 1.50$ MeV (b).

in the collective space, with $q^{(\min)}$ the value of $\hat{Q}_N$ where scission has completed (=the actual scission point) and $q^{(\max)}$ the value corresponding to the precursor to scission. We note

TABLE II. Interval $I_q = [q^{(\min)}, q^{(\max)}]$ of scission configurations as obtained from the JCN analysis of ^{240}Pu as a function of the temperature T.

T (MeV)	$q^{(\min)}$	$q^{(\max)}$	T (MeV)	$q^{(\min)}$	$q^{(\max)}$
0.00	0.2	2.6	1.00	0.3	3.1
0.25	0.2	2.5	1.25	0.5	3.1
0.50	0.2	2.8	1.50	0.5	3.1
0.75	0.2	3.0	1.75	0.7	3.1

that the precursor value is relatively stable, especially at high temperatures, while the position of the scission point, which is constant up to $T = 1.0$ MeV, moves to thicker necks beyond $T > 0.75$ MeV. We return to this result in Sec. IV E.

The JCN also picked up an interesting "zippering effect" of the data sets (the proton and neutron densities) at large temperatures and low q_N values. This effect is illustrated in Fig. 5, which shows the JCN at $q_N = 0.2$ at both $T = 0.0$ MeV (top) and $T = 1.5$ MeV (bottom). In both cases, the fragments are clearly formed, as evidenced by the two distinct branches in the upper right side of each figure. In addition, we notice at $T = 1.5$ MeV a complex pattern connecting the two fragments, which look similar to a zipper. We have found that this pattern becomes more noticeable for $T \geqslant 1.25$ MeV. Because the zippering connects the two prefragments, it should be indicative of a spatial connection between these two distinct regions of space; in addition, the effect manifests itself only at temperatures where the coupling to the continuum becomes sizable (see Sec. IV D). Therefore, we suggest that the zippering effect of the JCN is the representation of a spatial delocalization of quasiparticles (mostly neutrons) at large temperatures.

B. Quasiparticle occupations

The generalization at $T > 0$ of the procedure to identify a left fragment and a right fragment, their observables and their interaction energy presented in (I) is straightforward. Using the definition (9) for the one-body density matrix at finite temperature $T > 0$, we find that the coordinate space representation $\rho_\mu(\boldsymbol{r}\sigma,\boldsymbol{r}'\sigma')$ of the density of a single qp μ reads

$$\rho_\mu(\boldsymbol{r}\sigma,\boldsymbol{r}'\sigma') = \sum_{ij}[V^*_{i\mu}(1-f_\mu)V_{j\mu} + U_{i\mu}f_\mu U^*_{j\mu}] \times \phi_i(\boldsymbol{r}\sigma)\phi^*_j(\boldsymbol{r}'\sigma'), \quad (15)$$

with $\phi_i(\boldsymbol{r}\sigma)$ the single-particle basis functions. With this definition, the spatial occupation N_μ of the qp μ and the total number of particles N are formally the same as at $T = 0$; that is,

$$N_\mu = \sum_\sigma \int d^3\boldsymbol{r}\ \rho_\mu(\boldsymbol{r}\sigma,\boldsymbol{r}\sigma), \quad (16)$$

and

$$N_\mu = \sum_i [V^*_{i\mu}(1-f_\mu)V_{i\mu} + U_{i\mu}f_\mu U^*_{i\mu}]. \quad (17)$$

As in (I), we introduce the quantity

$$d_{ij}(z) = \sum_\sigma \int_{-\infty}^{+\infty} dx \int_{-\infty}^{+\infty} dy \int_{-\infty}^{z} dz\ \phi_i(\boldsymbol{r}\sigma)\phi^*_j(\boldsymbol{r}\sigma). \quad (18)$$

Still assuming that the neck between the two fragments is located on the z axis of the intrinsic reference frame and thus has the coordinates $\boldsymbol{r}_{\rm neck} = (0,0,z_N)$, we can define the occupation of the qp in the fragment (1) as

$$N_{1,\mu} = \sum_{ij}[V^*_{i\mu}(1-f_\mu)V_{j\mu} + U_{i\mu}f_\mu U^*_{j\mu}]d_{ij}(z_N). \quad (19)$$

As at $T = 0$, the occupation of the qp in the fragment (2) is simply $N_{2,\mu} = N_\mu - N_{1,\mu}$. We then assign the qp μ to fragment (1) if $N_{1,\mu} \geqslant 0.5N_\mu$ and to fragment (2) if $N_{1,\mu} < 0.5N_\mu$. This gives us two sets of quasiparticles. For each of them, we can define the corresponding pseudodensities and pseudopairing tensor. For fragment (f) we find, in coordinate $\otimes$ spin space,

$$\rho^{(\mathrm{f})}(\boldsymbol{r}\sigma,\boldsymbol{r}'\sigma') = \sum_{\mu\in(f)}\sum_{ij}[V^*_{i\mu}(1-f_\mu)V_{j\mu} + U_{i\mu}f_\mu U^*_{j\mu}]\phi_i(\boldsymbol{r}\sigma)\phi^*_j(\boldsymbol{r}'\sigma'), \quad (20)$$

$$\kappa^{(\mathrm{f})}(\boldsymbol{r}\sigma,\boldsymbol{r}'\sigma') = \sum_{\mu\in(f)}\sum_{ij}[V^*_{i\mu}(1-f_\mu)U_{j\mu} + U_{i\mu}f_\mu V^*_{j\mu}]\phi_i(\boldsymbol{r}\sigma)\phi^*_j(\boldsymbol{r}'\sigma'). \quad (21)$$

These are the equivalent at $T > 0$ of Eqs. (12) and (13) in (I). We can build the analog of the kinetic energy density and the spin current tensor from these pseudodensities. The Coulomb and nuclear interaction energy between the two fragments thus takes the same form as at $T = 0$; only the definition of the various pseudodensities is modified according to Eq. (9) and Eq. (20).

C. Quantum localization at finite temperature

As recalled in (I), at $T = 0$ the localization method of Ref. [72] is based on the idea that any unitary transformation of the qp operators $(\beta^\dagger,\beta)$ leaves the generalized density matrix, hence, all global observables such as the total energy, radii, etc., invariant. In this section, we generalize this result at $T > 0$ and discuss how it impacts the practical implementation of the method.

1. *Unitary transformation of quasiparticles*

As in (I), we consider the following unitary transformation $\hat{T}$ of the eigenvectors of the HFB matrix,

$$A_\alpha \equiv \hat{T}U_\mu = \sum_\mu T_{\alpha\mu}U_\mu, \quad (22)$$

$$B_\alpha \equiv \hat{T}V_\mu = \sum_\mu T_{\alpha\mu}V_\mu \quad (23)$$

where the quantities A_α, B_α, U_μ, and V_μ are, in fact, vectors with N components $A_{n\alpha}$ in the original sp basis, so that, in matrix form,

$$A = UT^T, \quad B = VT^T. \quad (24)$$

It is straightforward to notice that the matrix $\mathcal{W}'$, defined as

$$\mathcal{W}' = \begin{pmatrix} A & B^* \\ B & A^* \end{pmatrix} = \begin{pmatrix} U & V^* \\ V & U^* \end{pmatrix}\mathcal{T}^\dagger = \mathcal{W}\mathcal{T}^\dagger, \quad (25)$$

with

$$\mathcal{T} = \begin{pmatrix} T^* & 0 \\ 0 & T \end{pmatrix}, \quad \mathcal{T}\mathcal{T}^\dagger = \mathcal{T}^\dagger\mathcal{T} = 1, \quad (26)$$

verifies $\mathcal{W}'\mathcal{W}'^\dagger = \mathcal{W}'^\dagger\mathcal{W}' = 1$. The matrices A and B thus define new sets of qp operators $(\eta^\dagger,\eta)$ such that

$$\eta_\alpha = \sum_\mu T^*_{\alpha\mu}\beta_\mu, \quad \eta^\dagger_\alpha = \sum_\mu T_{\alpha\mu}\beta^\dagger_\mu. \quad (27)$$

Therefore, a unitary transformation of the Bogoliubov matrices of the type (22) and (23) correspond to a transformation of the qp creation (annihilation) operators into linear combination of themselves without mixing creation and annihilation operators [13].

With the help of the the Baker-Campbell-Hausdorff formula, it is not very difficult to show that, for the form (27) of the unitary transformation, there exists in Fock space a general transformation rule for the qp operators,

$$\eta_\mu = e^{i\hat{R}}\beta_\mu e^{-i\hat{R}}, \quad \eta^\dagger_\mu = e^{i\hat{R}}\beta^\dagger_\mu e^{-i\hat{R}}, \quad (28)$$

where $\hat{R}$ is a one-body Hermitian operator written in the original qp basis as $\hat{R} = \sum_{\mu\nu} R_{\mu\nu}\beta^\dagger_\mu\beta_\nu$.

2. *General invariance of the density matrix at $T > 0$*

We now prove that the one-body density matrix ρ_{ij} of Eq. (9) is invariant under a rotation of the qp operators. More precisely, if we start from a HFB vacuum corresponding to the rotated qp operators η and compute the one-body density matrix by using the Bogoliubov transformation $\mathcal{W}'$, the result is the same as if we had started from the HFB vacuum of the β operators using the initial Bogoliubov transformation $\mathcal{W}$.

The statistical trace defining ρ_{ij} can be computed in any arbitrary many-body basis $|n\rangle$ of the Fock space. Generically, we thus have

$$\rho_{ij} = \sum_n \langle n|\hat{D}c^\dagger_j c_i|n\rangle. \quad (29)$$

Let us introduce the new set of qp operators η obtained by the unitary transformation of Eq. (27). We choose the multi-qp states $|n\rangle$ of Eq. (29) from the vacuum of the rotated qp operators; that is,

$$|n\rangle \equiv |\eta_n\rangle = \eta^\dagger_1\cdots\eta^\dagger_n|\mathrm{vac}_\eta\rangle. \quad (30)$$

Then we introduce the Bogoliubov transformation $\mathcal{W}'$ to express the c operators as a function of the η operators. We find

$$\rho_{ij} = \sum_{\mu\nu} B_{j\mu}B^*_{i\nu}\sum_n\langle\eta_n|\hat{D}\eta_\mu\eta^\dagger_\nu|\eta_n\rangle + \sum_{\mu\nu}A^*_{j\mu}A_{i\nu}\sum_n\langle\eta_n|\hat{D}\eta^\dagger_\mu\eta_\nu|\eta_n\rangle. \quad (31)$$

We now use the property (28) to express the multi-qp states $|\eta_n\rangle$ of the η operators as a function of the multi-qp states $|\beta_n\rangle$ of the β operators. By definition of the multi-qp states, we find

$$|\eta_n\rangle = \eta^\dagger_1\cdots\eta^\dagger_n|\mathrm{vac}_\eta\rangle = e^{i\hat{R}}|\beta_n\rangle. \quad (32)$$

Above, we have the used the property $e^{-i\hat{R}}|\mathrm{vac}_\eta\rangle = |\mathrm{vac}_\beta\rangle$. This property is the direct consequence of the definition of the vacuum: It is the state such that, for all vectors v of the Fock space and any index i, $\langle v|\eta_i|\mathrm{vac}_\eta\rangle = 0$. Defining $|w\rangle = e^{-i\hat{R}}|v\rangle$, we find $\langle w|\beta_i e^{-i\hat{R}}|\mathrm{vac}_\eta\rangle = 0$. Hence, $e^{-i\hat{R}}|\mathrm{vac}_\eta\rangle$ is the vacuum for operators β_i, because the property is valid for all $|w\rangle$. Because the vacuum is unique, we must have $e^{-i\hat{R}}|\mathrm{vac}_\eta\rangle = |\mathrm{vac}_\beta\rangle$. In matrix form, we can thus write

$$\rho = B^*G'B^T + AF'A^\dagger \quad (33)$$

if we note

$$\begin{aligned} G' : G'_{\nu\mu} &= \sum_n \langle\beta_n|e^{-i\hat{R}}\hat{D}\eta_\mu\eta^\dagger_\nu e^{i\hat{R}}|\beta_n\rangle, \\ F' : F'_{\nu\mu} &= \sum_n \langle\beta_n|e^{-i\hat{R}}\hat{D}\eta^\dagger_\mu\eta_\nu e^{i\hat{R}}|\beta_n\rangle. \end{aligned} \tag{34}$$

By virtue of Eq. (27),

$$\begin{aligned} G'_{\nu\mu} &= \sum_{\alpha\beta} T^*_{\mu\alpha}T_{\nu\beta}\sum_n \langle\beta_n|e^{-i\hat{R}}\hat{D}\beta_\alpha\beta^\dagger_\beta e^{i\hat{R}}|\beta_n\rangle, \\ F'_{\nu\mu} &= \sum_{\alpha\beta} T_{\mu\alpha}T^*_{\nu\beta}\sum_n \langle\beta_n|e^{-i\hat{R}}\hat{D}\beta^\dagger_\alpha\beta_\beta e^{i\hat{R}}|\beta_n\rangle. \end{aligned} \tag{35}$$

In matrix form, this leads to

$$G' = TGT^\dagger, \quad F' = T^*FT^T, \tag{36}$$

with

$$\begin{aligned} G : G_{\beta\alpha} &= \sum_n \langle\beta_n|e^{-i\hat{R}}\hat{D}\beta_\alpha\beta^\dagger_\beta e^{i\hat{R}}|\beta_n\rangle, \\ F : F_{\beta\alpha} &= \sum_n \langle\beta_n|e^{-i\hat{R}}\hat{D}\beta^\dagger_\alpha\beta_\beta e^{i\hat{R}}|\beta_n\rangle. \end{aligned} \tag{37}$$

Putting everything back together, we find

$$\rho = B^*G'B^T + AF'A^\dagger, \tag{38}$$

$$= V^*T^\dagger TGT^\dagger TV^T + UT^TT^*FT^TT^*U^\dagger, \tag{39}$$

$$= V^*GV^T + UFU^\dagger. \tag{40}$$

Now it suffices to notice that

$$G_{\beta\alpha} = \mathrm{Tr}(e^{-i\hat{R}}\hat{D}\beta_\alpha\beta^\dagger_\beta e^{i\hat{R}}) = (1-f_\alpha)\delta_{\alpha\beta}, \tag{41}$$

by cyclic invariance of the trace. Similarly, we find that $F_{\beta\alpha} = f_\alpha\delta_{\alpha\beta}$, so that

$$\rho_{ij} = \sum_\alpha V_{j\alpha}V^*_{i\alpha}(1-f_\alpha) + \sum_\alpha U^*_{j\alpha}U_{i\alpha}f_\alpha. \tag{42}$$

This shows that the one-body density matrix in the single-particle basis is invariant under a unitary transformation of quasiparticle operators among themselves at $T > 0$. Equation (33) gives the expression of the density matrix after rotation of the qp; Eq. (9) gives the expression of the density matrix before rotation. Both expressions coincide. Using similar reasoning, one can show that the pairing tensor is also invariant under a unitary transformation. This implies that both the generalized density $\mathcal{R}$ and the HFB matrix (in the sp basis) are invariant, $\mathcal{R}' = \mathcal{R}$ and $\mathcal{H}' = \mathcal{H}$. Because the Wick theorem guarantees that there is a one-to-one correspondence between $\mathcal{R}$ and the quadratic operator $\hat{K}$ defining the density operator (see Sec. II B), we have also $\hat{K}' = \hat{K}$, and most importantly $\mathcal{H}' = \hat{K}'$. In other words, the HFB equations are still obeyed in the rotated qp basis.

3. *Quantum localization in the rotated quasiparticle basis*

Although the generalized density $\mathcal{R}$ in the sp basis is invariant under a unitary transformation of the qp, its form in the basis of the η operators (the rotated qp basis) is different from what it is in the basis of the β operators (the original qp basis). Before rotation, the matrix $\tilde{\mathcal{R}}$ of the generalized density in the quasiparticle basis is diagonal and we have the usual relations

$$\mathcal{R} = \mathcal{W}\tilde{\mathcal{R}}\mathcal{W}^\dagger, \quad \tilde{\mathcal{R}} = \begin{pmatrix} f & 0 \\ 0 & 1-f \end{pmatrix}. \tag{43}$$

Introducing the unitary transformation $\mathcal{T}$, we can write

$$\mathcal{R} = \mathcal{W}'\begin{pmatrix} T^* & 0 \\ 0 & T \end{pmatrix}\begin{pmatrix} f & 0 \\ 0 & 1-f \end{pmatrix}\begin{pmatrix} T^T & 0 \\ 0 & T^\dagger \end{pmatrix}\mathcal{W}'^\dagger. \tag{44}$$

Owing to Eq. (36), we can define the matrix of the generalized density in the new qp basis of the η operators defined by Eq. (27) with

$$\tilde{\mathcal{R}}' = \begin{pmatrix} T^* & 0 \\ 0 & T \end{pmatrix}\begin{pmatrix} f & 0 \\ 0 & 1-f \end{pmatrix}\begin{pmatrix} T^T & 0 \\ 0 & T^\dagger \end{pmatrix}. \tag{45}$$

In our case, the unitary transformation is given by definition (23) in (I),

$$T = \begin{pmatrix} \cos\theta & \sin\theta \\ -\sin\theta & \cos\theta \end{pmatrix}. \tag{46}$$

A simple calculation yields, for the pair (μ,ν) of quasiparticles,

$$\begin{aligned} T^*\begin{pmatrix} f_\mu & 0 \\ 0 & f_\nu \end{pmatrix}T^T = \begin{pmatrix} f_\mu & 0 \\ 0 & f_\nu \end{pmatrix} - \sin\theta(f_\mu - f_\nu) \\ \times \begin{pmatrix} \sin\theta & \cos\theta \\ \cos\theta & -\sin\theta \end{pmatrix}, \end{aligned} \tag{47}$$

and a similar expression for the term $1-f$. Therefore, the generalized density matrix loses its diagonal form up to first order in $\Delta f = f_\mu - f_\nu$. In the rotated qp basis, the generalized density thus takes the generic form

$$\tilde{\mathcal{R}}' = \begin{pmatrix} f_k & & & & & & \\ & \ddots & & & & & \\ & & F_{\mu\mu} & F_{\mu\nu} & & & \\ & & F_{\nu\mu} & F_{\nu\nu} & & & \\ & & & & 1-f_k & & \\ & & & & & \ddots & \\ & & & & & & G_{\mu\mu} \quad G_{\mu\nu} \\ & & & & & & G_{\nu\mu} \quad G_{\nu\nu} \end{pmatrix}. \tag{48}$$

It can always be ordered in the form of a block-diagonal matrix, with exactly diagonal terms that contain the statistical occupations of the qp that have not been rotated and 2×2 nondiagonal blocks corresponding to each pair (μ,ν) of rotated qp.

As a consequence of the nondiagonal form of $\tilde{\mathcal{R}}'$, the one-body density matrix cannot be expressed as a simple sum over single qp densities. This implies that the coordinate space representation of ρ becomes

$$\rho(\boldsymbol{r}\sigma,\boldsymbol{r}'\sigma') = \sum_{k\in\mathcal{S}} \rho_k(\boldsymbol{r}\sigma,\boldsymbol{r}'\sigma') + \sum_{\mu\nu\in\mathcal{P}} \rho'_{\mu\nu}(\boldsymbol{r}\sigma,\boldsymbol{r}'\sigma'), \quad (49)$$

where $\mathcal{S}$ refers to the set of qps that are not rotated, and $\mathcal{P}$ to the set of qps that are rotated. The contribution $\rho'_{\mu\nu}(\boldsymbol{r}\sigma,\boldsymbol{r}'\sigma')$ of the rotated pair (μ,ν) of qps to the total one-body density (which is invariant) is

$$\begin{aligned}\rho'_{\mu\nu}(\boldsymbol{r}\sigma,\boldsymbol{r}'\sigma') = \sum_{ij} \phi_i(\boldsymbol{r}\sigma)\phi^*_j(\boldsymbol{r}'\sigma')[&B^*_{i\mu}G'_{\mu\mu}B_{j\mu} \\ &+ A_{i\mu}F'_{\mu\mu}A^*_{j\mu} + B^*_{i\mu}G'_{\mu\nu}B_{j\nu} + A_{i\mu}F'_{\mu\nu}A^*_{j\nu} \\ &+ B^*_{i\nu}G'_{\nu\mu}B_{j\mu} + A_{i\nu}F'_{\nu\mu}A^*_{j\mu} + B^*_{i\nu}G'_{\nu\nu}B_{j\nu} \\ &+ A_{i\nu}F'_{\nu\nu}A^*_{j\nu}]. \end{aligned} \quad (50)$$

For rotated qps, the notion of spatial occupation cannot be captured by the quantity N_μ alone. We thus redefine the spatial occupation of the rotated pairs (μ,ν) and (ν,μ) of quasiparticles by

$$\begin{aligned} N'_{\mu\nu} = &\sum_i [B^*_{i\mu}G'_{\mu\mu}B_{i\mu} + A_{i\mu}F'_{\mu\mu}A^*_{i\mu}] \\ &+ \sum_i [B^*_{i\mu}G'_{\mu\nu}B_{i\nu} + A_{i\mu}F'_{\mu\nu}A^*_{i\nu}] \end{aligned} \quad (51)$$

and

$$\begin{aligned} N'_{\nu\mu} = &\sum_i [B^*_{i\nu}G'_{\nu\nu}B_{i\nu} + A_{i\nu}F'_{\nu\nu}A^*_{i\nu}] \\ &+ \sum_i [B^*_{i\nu}G'_{\nu\mu}B_{i\mu} + A_{i\nu}F'_{\nu\mu}A^*_{i\mu}]. \end{aligned} \quad (52)$$

Note that $N'_{\mu\nu} \neq N'_{\nu\mu}$. A tedious but straightforward calculation shows that $N'_{\mu\nu} + N'_{\nu\mu} = N_\mu + N_\nu$, which is nothing but the consequence of the invariance of the density matrix under this rotation. Similarly, the spatial occupations in the fragment (1) of the rotated pair (μ,ν) and (ν,μ) of quasiparticles now read

$$\begin{aligned} N'_{1,\mu\nu} = &\sum_{ij} [B^*_{i\mu}G'_{\mu\mu}B_{j\mu} + A_{i\mu}F'_{\mu\mu}A^*_{j\mu}]d_{ij}(z_N) \\ &+ \sum_{ij} [B^*_{i\mu}G'_{\mu\nu}B_{j\nu} + A_{i\mu}F'_{\mu\nu}A^*_{j\nu}]d_{ij}(z_N) \end{aligned} \quad (53)$$

and

$$\begin{aligned} N'_{1,\nu\mu} = &\sum_{ij} [B^*_{i\nu}G'_{\nu\nu}B_{j\nu} + A_{i\nu}F'_{\nu\nu}A^*_{j\nu}]d_{ij}(z_N) \\ &+ \sum_{ij} [B^*_{i\nu}G'_{\nu\mu}B_{j\mu} + A_{i\nu}F'_{\nu\mu}A^*_{j\mu}]d_{ij}(z_N). \end{aligned} \quad (54)$$

This simple extension reflects the fact that the two qps forming the pair are not independent anymore.

To finish this section, we note that the HFB matrix, just like the generalized density, is not diagonal in the rotated qp basis. This situation already occurred at $T = 0$ [30]. Because of this property, special attention should be paid before extending the formalism to account, e.g., for low-lying excitations using the qp random phase approximation (QRPA). In the rotated qp basis, the QRPA equations would take a form that is different from usual.

4. Implementation of the quantum localization at $T > 0$

In practice, we construct the fission fragments by scanning both the set $\mathcal{S}$ of nonrotated qps and the set $\mathcal{P}$ of rotated qps.

(i) For all qps $\mu \in \mathcal{S}$, we compute N_μ, $N_{1,\mu}$, and $N_{2,\mu}$ according to Eqs. (17) and (19); the qp is assigned to fragment (1) if $N_{1,\mu} \geqslant 0.5N_\mu$, to fragment (2) otherwise.

(ii) Let us note $\mathcal{P}_\mu = (\mu,\nu)$ the pair of qps μ and ν. We have $\mathcal{P} = \bigcup \mathcal{P}_\mu$. For each pair $\mathcal{P}_\mu$, and for each qp μ in this pair, we compute $N'_{\mu\nu}$, $N'_{1,\mu\nu}$, and $N'_{2,\mu\nu}$ according to Eqs. (51)–(54); the qp μ is assigned to fragment (1) if $N'_{1,\mu\nu} \geqslant 0.5N'_{\mu\nu}$, to fragment (2) otherwise. Note that the procedure must be done separately for the qp μ of and the qp ν of the pair, because $N'_{\mu\nu} \neq N'_{\nu\mu}$.

The result of this procedure is to partition the whole set of quasiparticles into two subsets corresponding to the two fragments. The pseudodensities in the fragment can then be formally written as

$$\begin{aligned} \rho'^{(\mathrm{f})}(\boldsymbol{r}\sigma,\boldsymbol{r}'\sigma') = &\sum_{\mu\in(f)} \sum_{\nu\in\mathcal{P}_\mu} \sum_{ij} [B^*_{i\mu}G'_{\mu\nu}B_{j\nu} \\ &+ A_{i\mu}F'_{\mu\nu}A^*_{j\mu}]\phi_i(\boldsymbol{r}\sigma)\phi^*_j(\boldsymbol{r}'\sigma'), \end{aligned} \quad (55)$$

$$\begin{aligned} \kappa'^{(\mathrm{f})}(\boldsymbol{r}\sigma,\boldsymbol{r}'\sigma') = &\sum_{\mu\in(f)} \sum_{\nu\in\mathcal{P}_\mu} \sum_{ij} [B^*_{i\mu}G'_{\mu\nu}A_{j\nu} \\ &+ A_{i\mu}F'_{\mu\nu}B^*_{j\nu}]\phi_i(\boldsymbol{r}\sigma)\phi^*_j(\boldsymbol{r}'\sigma'). \end{aligned} \quad (56)$$

These relations make it possible to extend the calculation of the interaction energy between the fragments and the fragment internal energies at $T > 0$ using the formulas given in (I).

We have implemented the localization method in a new module of the DFT solver HFODD [57]. The rotation of the qp is first performed in the sp space; i.e., the matrices U and V of the Bogoliubov transformation are rotated according to Eq. (25). Using Eqs. (9) and (33), we have checked that the density matrix in the sp basis (the deformed HO basis in our case) remains invariant after the transformation within numerical precision.

In HFODD, calculations of the nuclear and Coulomb interaction energy are carried out in coordinate space. The matrices of the Bogoliubov transformation are first transformed into spinors according to

$$\begin{aligned} \varphi^{(1)}_\mu(\boldsymbol{r}\sigma) &= -2\sigma \sum_i U^*_{i\mu}\phi^*_i(\boldsymbol{r}-\sigma), \\ \varphi^{(2)}_\mu(\boldsymbol{r}\sigma) &= \sum_i V^*_{i\mu}\phi_i(\boldsymbol{r}\sigma). \end{aligned} \quad (57)$$

Note that this transformation depends on a specific phase convention. Local densities are then defined in terms of these HFB spinors; see Ref. [73] for details. We have then checked

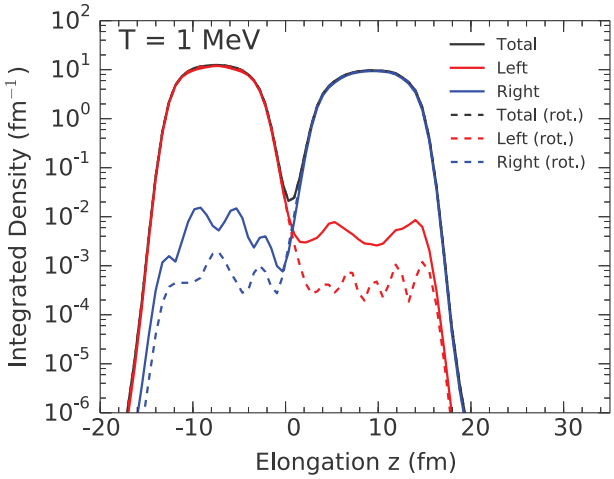

FIG. 6. (Color online) Profile of the integrated nuclear density $\rho(z)$ (integrated over x and y coordinates) along the elongation axis z in ^{240}Pu at $q_N = 0.7$ and $T = 1.0$ MeV before (solid lines) and after (dashed lines) rotation of the qp wave functions.

that the coordinate space representations of the densities, as computed from the HFB spinors (57), are also invariant after the qp rotation within machine precision.

As an example, Fig. 6 shows the impact of the localization on the pseudodensities of the fission fragments. The figure shows the one-body density matrix of the compound nucleus before and after rotation; it also shows the pseudodensities of the left and right fragments, before and after rotation. All densities were integrated along the x and y directions. As at $T = 0$, we observe a significant decrease of the tails of the densities, of approximately an order of magnitude. The curves labeled "Total" and "Total (rot.)," which pertain to the total density before and after rotation, are indistinguishable.

D. Coupling to the continuum

It was demonstrated in Refs. [49,50] based on the coordinate space formulation of the HFB equations (in spherical symmetry) that the asymptotic conditions for the (U,V) matrices of the Bogoliubov transformations read

$$U(E,r\sigma) \to \begin{cases} \cos(k_1 r + \delta_1), & E > -\lambda, \\ e^{-\kappa_1 r}, & E < -\lambda, \end{cases} \tag{58}$$

$$V(E,r\sigma) \to \begin{cases} \cos(k_1 r + \delta_1), & E < +\lambda, \\ e^{-\kappa_1 r}, & E > +\lambda. \end{cases} \tag{59}$$

From these expressions, it was shown that for nuclei with negative Fermi energy, the local density is always localized, which leads to observables taking finite values.

At $T > 0$, the FT-HFB equations take exactly the same form as at $T = 0$; hence, the matrices U and V of the Bogoliubov transformation have the same asymptotic properties. We summarize in Table III the localized or delocalized nature of the U and V matrices of the Bogoliubov transformation depending on the value of the Fermi level λ and the energy E of the qp.

Contrary to the case at $T = 0$, however, the density matrix now takes the form of Eq. (9), and the additional term $fUU^\dagger$

TABLE III. Localization properties at $T > 0$ of the matrices (U,V) of the Bogoliubov transformation depending on the value of the qp energies and the Fermi level.

Fermi level	qp energy	Localization of (U,V)
$\lambda > 0$	$E > +\lambda$	U delocalized, V localized
	$E < +\lambda$	U delocalized, V delocalized
$\lambda < 0$	$E > -\lambda$	U delocalized, V localized
	$E < -\lambda$	U localized, V localized

can be delocalized even for systems with negative Fermi energy. In fact, the set of quasiparticles can be split into the subset $\mathcal{L}$ of localized, discrete qps, with $0 \leqslant E < -\lambda$, and the subset $\mathcal{C}$ of delocalized, continuous qps with $E > -\lambda$. The full density is, of course, the sum of the two contributions

$$\rho_{ij} = \rho_{ij}^{(\mathrm{loc})} + \rho_{ij}^{(\mathrm{con})}, \tag{60}$$

with

$$\rho_{ij}^{(\mathrm{loc})} = \sum_{\mu\in\mathcal{L}} [V_{i\mu}^*(1-f)_\mu V_{j\mu} + U_{i\mu} f_\mu U_{j\mu}^*] \tag{61}$$

and (assuming the continuous spectrum is discretized as, e.g., happens in the HO basis)

$$\rho_{ij}^{(\mathrm{con})} = \sum_{\mu\in\mathcal{C}} [V_{i\mu}^*(1-f)_\mu V_{j\mu} + U_{i\mu} f_\mu U_{j\mu}^*]. \tag{62}$$

In Fig. 7, we illustrate this result by showing the profile of the total isoscalar density $\rho_0(\boldsymbol{r})$ along the elongation axis of ^{240}Pu in the scission region, at $q_N = 1.0$, together with the contribution of the term $fUU^\dagger$ to its delocalized contribution $\rho_{ij}^{(\mathrm{con})}$. Curves are shown at $T = 1.0, 1.5$, and 2.0 MeV. At $T = 1.0$ MeV, the energy of the incident neutron is of the order of 25 MeV, while it is more than 70 MeV at $T = 2.0$ MeV. Yet, even at such a high excitation energy and after integrating over the transverse coordinates x and y, the contribution of

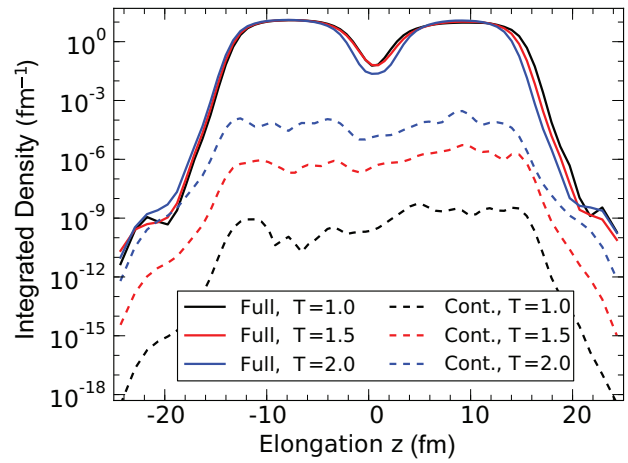

FIG. 7. (Color online) Profile of the isoscalar nuclear density $\rho_0(\boldsymbol{r})$ (integrated over x and y coordinates) along the elongation axis z in ^{240}Pu at $q_N = 1.0$ and $T = 1.0, 1.5$, and 2.0 MeV. The solid lines correspond to the full density; the dashed lines to the term $fUU^\dagger$ only of $\rho^{(\mathrm{con})}$.

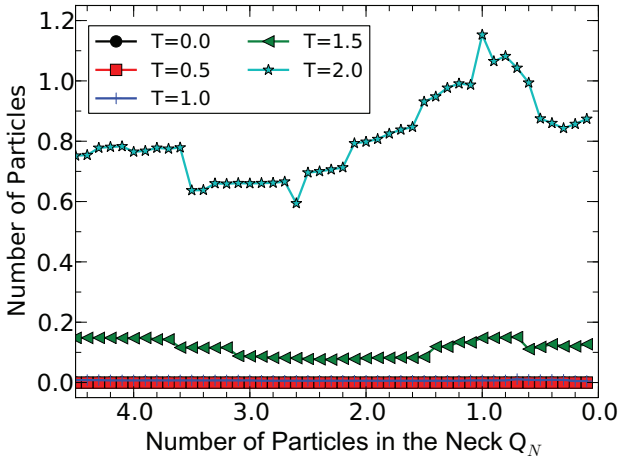

FIG. 8. (Color online) Total number of delocalized quasiparticles as a function of the number of particles in the neck for various temperatures.

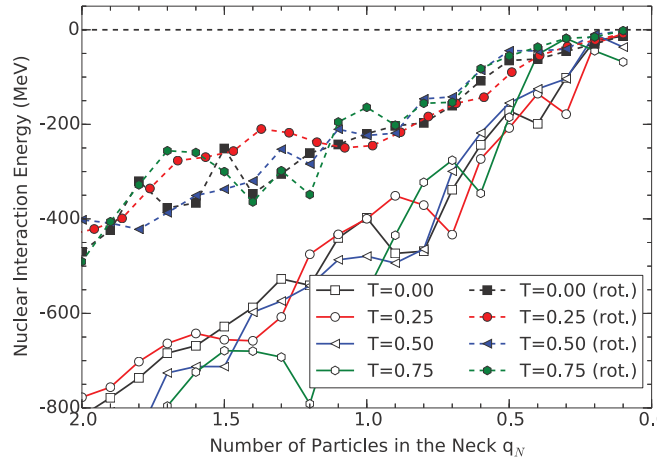

FIG. 9. (Color online) Skyrme interaction energy between the fission fragments of ^{240}Pu as a function of the number of particles in the neck for the SkM* functional at low temperatures $0.00 \leqslant T \leqslant 0.75$ MeV. Solid curves with open symbols correspond to the calculation before the localization is applied; dashed curves with solid symbols to the localized qp.

the term $fUU^{\dagger}$ to the total density is, at most, of the order of 10^{-4}. We note that the use of the one-center HO basis induces numerical limitations: The tails of the densities at the boundaries of the domain are not physical but a consequence of the Gaussian asymptotic behavior of the basis functions (which is visible as a roughly parabolic decrease of the density near $z = \pm 20$–25 fm).

The densities can be further integrated over z to provide an estimate of the number of particles originating from the qp located in the continuum. This is shown in Fig. 8 as a function of q_N for five values of the nuclear temperature, $T = 0, 0.5, \ldots, 2.0$ MeV. For temperatures below 1.5 MeV, the number of particles is virtually zero; only beyond 1.5 MeV is the contribution noticeable, with up to about 1 particle in the continuum at $T = 2.0$ MeV. Because of the unphysical spatial truncation of qp wave functions induced by the asymptotic behavior of the basis functions, it may be possible that the actual coupling to the continuum is a little stronger. It is, however, unlikely that the effect is strong enough to have a sizable impact on the physics of neutron-induced fission.

We have thus shown that, in the regime of temperatures relevant to the description of induced nuclear fission, the coupling to the continuum remains essentially negligible. Our results are fully compatible with estimates published in the literature. Indeed, early works in the context of the finite-temperature Hartree-Fock theory suggested that the effect of the continuum becomes significant only at $T > 4$ MeV [52]. In the follow-up paper by the same authors, the density of neutron vapor in ^{208}Pb was shown to be 0.510^{-2} fm $^{-3}$ at $T = 7$ MeV [51]. More recent estimates obtained at the fully FT-HFB level with a coordinate-space solver also suggest a total number of particles in the continuum of 0.2 at $T = 1.5$ MeV in the superheavy element $Z = 114$, $N = 178$ [25]. These results are noteworthy, because they justify *a posteriori* the validity of the model of the compound nucleus to describe induced fission.

E. Fragment interaction energy and kinetic energy

Based on the JCN analysis presented in Sec. IV A, we have identified the range $q_N \in [0.1$–$3.0]$ as the scission region, with $q_N \approx 0.2$–0.3 as the most likely scission point (at low temperatures). Using the generalized quantum localization procedure of Sec. IV C 3, we have computed the fission fragment interaction energy and total kinetic energy before and after localization for the range of temperatures $0 \leqslant T \leqslant 1.75$ MeV. For $T \geqslant 1.50$ MeV, the localization method begins to break down: On the one hand, the number of possible pairs meeting the criteria for rotation becomes very large and the procedure becomes very time-consuming; in addition, it does not always succeed in fully localizing the fragments. This may be an indirect effect of the coupling to the continuum discussed in the previous section.

It is interesting to distinguish two temperature regimes. In the range $0 \leqslant T \leqslant 0.75$ MeV, which is depicted in Fig. 9, there are relatively few qualitative differences between the zero-temperature case and the finite-temperature results: The nuclear interaction energy is of the same order of magnitude at all T, both before and after quantum localization. This is consistent with the earlier observation in Sec. III A that the PES does not change dramatically in this temperature range. As in (I), we note relatively large fluctuations of the interaction energy as a function of q_N, especially before localization. To a large extent, these fluctuations reflect the binary nature of the partitioning of the nucleus in two (entangled) fragments: A given qp could be assigned to one fragment for a given q_N and to the other at $q_N + \delta q_N$, especially if its localization ℓ indicator is close to 0.5. After localization, such fluctuations are strongly attenuated but do not disappear entirely, because there remain a few qps that can not be properly localized [72]. In addition, small discontinuities in the unconstrained collective variables can also contribute to the fluctuations of interaction energy.

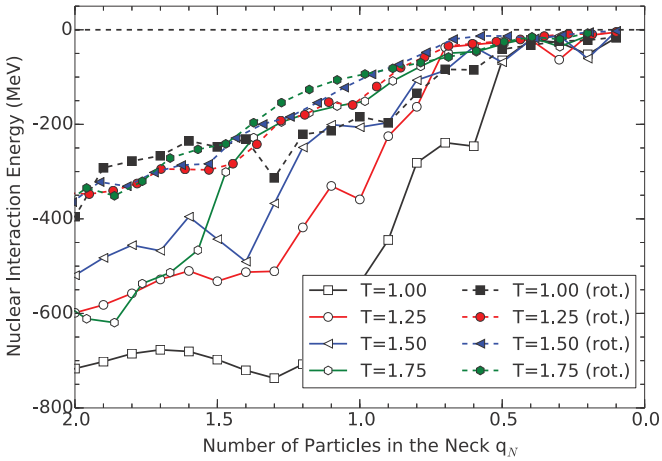

FIG. 10. (Color online) Same as Fig. 9 in the higher temperature regimes $1.00 \leqslant T \leqslant 1.75$ MeV.

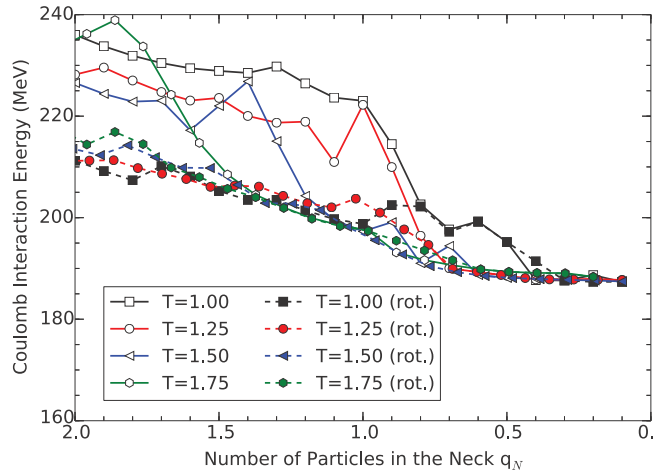

FIG. 12. (Color online) Same as Fig. 11 in the higher temperature range $1.00 \leqslant T \leqslant 1.75$ MeV.

In the higher temperature regime, the effect of changes in temperature becomes more visible (see Fig. 10). From a purely topological point of view, the scission point, as determined by the JCN, is pushed back from $q_N \approx 0.2$–0.4 to $q_N \approx 0.5$–0.9. This observation is confirmed by the behavior of the nuclear interaction energy: As a function of q_N, the interaction energy goes to zero faster as T increases. This trend is already clearly visible before localization, the effect of which is to make it more pronounced. Qualitatively, these results show that the system tends to break with a thicker neck than at lower temperatures, in a manner somewhat similar to glass.

We show in Fig. 11 the variations of the direct Coulomb interaction energy along the q_N trajectory at low temperatures, which are the most relevant to applications of neutron-induced fission. We notice again the smoothing effect of the localization method, especially at large q_N values, where the fragments are still heavily entangled. We also remark that the effect of the temperature is weak, which is compatible with experimental evidence, which shows a variation of about 2 MeV in total kinetic energy (TKE) over a 5-MeV range of neutron energies [74]. For $q_N = 0.2$, which the JCN analysis identifies as the most likely scission configuration, the Coulomb interaction energy seems first to increase with temperature, from about 185 MeV up to approximately 195 MeV at $T = 0.50$ MeV (corresponding to $E^* \approx 8$–10-MeV excitation energy in the compound nucleus), before decreasing as temperature keeps on increasing. However, it is clear from the figure that the amplitude of the energy fluctuations along the $\hat{Q}_N$ path in the scission region are quite large, so these results should be taken with a grain of salt.

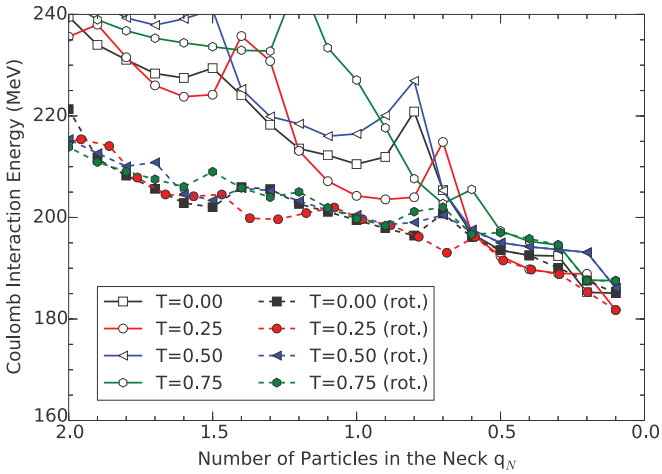

FIG. 11. (Color online) Direct Coulomb interaction energy in the fission of ^{240}Pu as a function of the number of particles in the neck for the SkM* functional for temperatures in the range $0.00 \leqslant T \leqslant 0.75$ MeV.

Finally, Fig. 12 shows the evolution of the direct Coulomb interaction energy along the $\hat{Q}_N$ path at higher temperatures $T \geqslant 1.00$ MeV. This corresponds to incident neutron energies larger than 25 MeV. In this regime, pairing correlations have vanished entirely. Quite surprisingly, the total Coulomb interaction energy is nearly constant at low q_N values, and this constant value is the same for all temperatures. Considering the large uncertainties of the current calculations, it is premature to draw definitive conclusions, but this point calls for further studies.

The calculations presented here are clearly schematic and have yet to reach the accuracy obtained from evaluations [74]. We recall that the goal of this paper is to set up a framework based on finite-temperature DFT that can be used in more systematic studies. In particular, it becomes clear from Figs. 9–12 that scission configurations must be identified from a PES that is fully continuous, which should remove some of the fluctuations observed here. This can be achieved by considering simultaneously all relevant collective variables, i.e., at least $\hat{Q}_{20}$, $\hat{Q}_{22}$, $\hat{Q}_{30}$, $\hat{Q}_{40}$, and $\hat{Q}_N$, together with the temperature. To compare theoretical predictions with experimental data, which is based on the average total kinetic energy, the local enlargement of the collective space should be repeated for all fragmentations observed in the ^{239}Pu(n, f) reaction. Improvements on the quantum localization methods are also possible. Work along these lines is currently under way.

V. CONCLUSIONS

One of the main challenges for a theory of induced fission is the need to accurately describe the (possibly high) excitation energy of the compound nucleus. In this paper, we have adopted the finite temperature nuclear density formalism to describe neutron-induced fission.

(i) We have validated the nuclear DFT framework at finite temperature for the description of induced fission. In particular, we have given a prescription to relate the excitation energy of the compound nucleus to the nuclear temperature of the FT-HFB theory. Following Ref. [25], we have confirmed the validity of the Maxwell relations of thermodynamics over the entire fission pathway, with the exception of the scission region (unless there are enough collective variables to make the PES continuous).

(ii) We have quantified the effect of the incident neutron energy on the fission barriers of the compound nucleus ^{240}Pu. In particular, we have found that fission barriers slightly increase in the energy range $E_n = 0$–5 MeV; at higher neutron energies, the trend is reversed and fission barriers decrease monotonically. We stress that, in the energy range of interest in applications of induced fission, ($E_n = 0$–14 MeV), the barriers are lower by at most 15%. While this can have a significant impact on fission observables, in particular fission probabilities, the effect is not as dramatic as may have been expected from, e.g., studies of cold fusion in superheavy nuclei [24].

(iii) We have given a microscopic foundation at $T > 0$ of the central hypothesis of induced fission as a two-step process based on the decay of a compound nucleus. Indeed, we have confirmed that the coupling to the continuum induced by the finite temperature is negligible at least up to 50 MeV of excitation energy ($T \approx 1.5$ MeV) and remain small even at larger excitation energies.

(iv) We have generalized the quantum localization method of Ref. [72] to the case of the finite temperature DFT, showing that the method remains applicable up to $T \approx 1.5$ MeV. We have found that scission tends to occur at larger values of the number of particles in the neck as temperature increases.

In principle, the finite temperature DFT framework should allow us to compute the excitation energy of the fragment in a fully microscopic way. There are, however, multiple caveats. First of all, we have seen that the position of the scission point changes with temperature. The charge and mass of the fission fragments also change: The evolution of a given fragment (Z,N) as a function of the excitation energy of the compound nucleus cannot be obtained from a single fission pathway only, but requires the full local scission hypersurface. An additional difficulty is that both the charge and the mass of the fragments are noninteger numbers, through both quantum and statistical fluctuations. Of course, we may perform HFB calculations for the fragments by imposing that $\langle\hat{Z}\rangle$ and $\langle\hat{N}\rangle$ take any value, including fractional ones, but it is not clear how accurate this approximation would be.

In this work, we have restricted ourselves to a static view of the fission process. A dynamical treatment of the process would certainly require an extension of the microscopic theory of collective inertia at finite temperature. This would allow both fully consistent computations of spontaneous fission half-lives in the commonly adopted WKB approximation and calculations of fission yields and energy distributions in the time-dependent generator coordinate method, such as in Refs. [34,35,75].

ACKNOWLEDGMENTS

Stimulating discussions with W. Younes, D. Gogny, D. Regnier, and J. Randrup are very gratefully acknowledged. We are also thankful to W. Nazarewicz and J. C. Pei for useful comments. This work was partly performed under the auspices of the U.S. Department of Energy by Lawrence Livermore National Laboratory under Contract No. DE-AC52-07NA27344. Funding was also provided by the U.S. Department of Energy Office of Science, Nuclear Physics Program, pursuant to Contract No. DE-AC52-07NA27344, Clause B-9999, Clause H-9999, and the American Recovery and Reinvestment Act, Pub. L. 111-5. Computational resources were provided through an INCITE grant, "Computational Nuclear Structure," by the National Center for Computational Sciences (NCCS) and National Institute for Computational Sciences (NICS) at Oak Ridge National Laboratory. Additional computing support was provided by the Livermore Computing Resource Center at Lawrence Livermore National Laboratory. Thanks are also due to the UK Engineering and Physical Sciences Research Council, under Grant No. EP/J013072/1.

[1] M. B. Chadwick *et al.*, ENDF/B-VII.1 nuclear data for science and technology: Cross sections, covariances, fission product yields and decay data, Nucl. Data Sheets **112**, 2887 (2011).

[2] B. E. Watt, Energy spectrum of neutrons from thermal fission of U^{235}, Phys. Rev. **87**, 1037 (1952).

[3] N. Bohr and J. A. Wheeler, The mechanism of nuclear fission, Phys. Rev. **56**, 426 (1939).

[4] A. Bohr and B. Mottelson, *Nuclear Structure*, Vol. II (Benjamin, New York, 1975).

[5] T. Duguet, M. Bender, K. Bennaceur, D. Lacroix, and T. Lesinski, Particle-number restoration within the energy density functional formalism: Nonviability of terms depending on noninteger powers of the density matrices, Phys. Rev. C **79**, 044320 (2009).

[6] D. Lacroix, T. Duguet, and M. Bender, Configuration mixing within the energy density functional formalism: Removing spurious contributions from nondiagonal energy kernels, Phys. Rev. C **79**, 044318 (2009).

[7] M. Bender, K. Bennaceur, T. Duguet, P.-H. Heenen, T. Lesinski, and J. Meyer, Tensor part of the Skyrme energy density functional. II. deformation properties of magic and semi-magic nuclei, Phys. Rev. C **80**, 064302 (2009).

[8] M. V. Stoitsov, J. Dobaczewski, R. Kirchner, W. Nazarewicz, and J. Terasaki, Variation after particle-number projection for the Hartree-Fock-Bogoliubov method with the Skyrme energy density functional, Phys. Rev. C **76**, 014308 (2007).

[9] M. Anguiano, J. L. Egido, and L. M. Robledo, Particle number projection with effective forces, Nucl. Phys. A **696**, 467 (2001).

[10] R. Bernard, H. Goutte, D. Gogny, and W. Younes, Microscopic and nonadiabatic Schrödinger equation derived from the generator coordinate method based on zero- and two-quasiparticle states, Phys. Rev. C **84**, 044308 (2011).

[11] R. Eschrig, *Fundamentals of Density Functional Theory* (Teubner, Leipzig, 1996).

[12] R. Parr and W. Yang, *Density Functional Theory of Atoms and Molecules* (Oxford University Press, Oxford, UK, 1989).

[13] J.-P. Blaizot and G. Ripka, *Quantum Theory of Finite Systems* (MIT Press, Cambridge, MA, 1985).

[14] J. des Cloizeaux, in Approximation de Hartree-Fock et approximation de phase aléatoire à température finie, *Many-Body Physics*, edited by C. DeWitt and R. Balian (Gordon and Breach Science Publishers, Philadelphia, 1968).

[15] F. Garcias, M. Barranco, A. Faessler, and N. Ohtsuka, Angular momentum and temperature dependence of fission barriers with a realistic force, Z. Physik A **336**, 31 (1990).

[16] F. Garcias, M. Barranco, J. Nemeth, C. Ngô, and X. Viñas, The fission of hot rotating nuclei: A selfconsistent Thomas-Fermi calculation, Nucl. Phys. A **495**, 169 (1989).

[17] C. Guet, E. Strumberger, and M. Brack, Liquid drop parameters for hot nuclei, Phys. Lett. B **205**, 427 (1988).

[18] D. Dalili, J. Németh, and C. Ngô, A self consistent Thomas-Fermi calculation of fission barriers at finite temperature and angular momentum as applied to the ^{205}At, Z. Physik A **321**, 335 (1985).

[19] J. Nemeth, D. Dalili, and C. Ngô, Hartree-Fock and Thomas-Fermi self-consistent calculations of the ^{144}Nd nucleus at finite temperature and angular momentum, Phys. Lett. B **154**, 11 (1985).

[20] M. Diebel, K. Albrecht, and R. W. Hasse, Microscopic calculations of fission barriers and critical angular momenta for excited heavy nuclear systems, Nucl. Phys. A **355**, 66 (1981).

[21] J. Bartel, M. Brack, and M. Durand, Extended Thomas-Fermi theory at finite temperature, Nucl. Phys. A **445**, 263 (1985).

[22] M. Brack and P. Quentin, Selfconsistent calculations of highly excited nuclei, Phys. Lett. B **52**, 159 (1974).

[23] J. Mcdonnell, N. Schunck, and W. Nazarewicz, Microscopic description of nuclear fission: Fission barrier heights of even-even actinides, *Fission and Properties of Neutron-Rich Nuclei* (World Scientific, Sanibel Island, FL, 2013), p. 597.

[24] J. A. Sheikh, W. Nazarewicz, and J. C. Pei, Systematic study of fission barriers of excited superheavy nuclei, Phys. Rev. C **80**, 011302 (2009).

[25] J. C. Pei, W. Nazarewicz, J. A. Sheikh, and A. K. Kerman, Fission barriers of compound superheavy nuclei, Phys. Rev. Lett. **102**, 192501 (2009).

[26] S. Hilaire, M. Girod, S. Goriely, and A. J. Koning, Temperature-dependent combinatorial level densities with the D1M Gogny force, Phys. Rev. C **86**, 064317 (2012).

[27] J. L. Egido, L. M. Robledo, and V. Martin, Behavior of shell effects with the excitation energy in atomic nuclei, Phys. Rev. Lett. **85**, 26 (2000).

[28] J. L. Egido and P. Ring, The decay of hot nuclei, J. Phys. G: Nucl. Part. Phys. **19**, 1 (1993).

[29] J. L. Egido, Quantum versus statistical fluctuations in mean-field theories, Phys. Rev. Lett. **61**, 767 (1988).

[30] N. Schunck, D. Duke, H. Carr, and A. Knoll, Description of induced nuclear fission with Skyrme energy functionals: Static potential energy surfaces and fission fragment properties, Phys. Rev. C **90**, 054305 (2014).

[31] M. Bender, P.-H. Heenen, and P.-G. Reinhard, Self-consistent mean-field models for nuclear structure, Rev. Mod. Phys. **75**, 121 (2003).

[32] P. Ring and P. Schuck, *The Nuclear Many-Body Problem* (Springer-Verlag, Berlin, 2000).

[33] W. Younes and D. Gogny, Fragment yields calculated in a time-dependent microscopic theory of fission, Technical Report LLNL-TR-586678, Lawrence Livermore National Laboratory (LLNL), Livermore, CA, 2012.

[34] H. Goutte, J. F. Berger, P. Casoli, and D. Gogny, Microscopic approach of fission dynamics applied to fragment kinetic energy and mass distributions in ^{238}U, Phys. Rev. C **71**, 024316 (2005).

[35] J. F. Berger, M. Girod, and D. Gogny, Constrained Hartree-Fock and beyond, Nucl. Phys. A **502**, 85 (1989).

[36] J. Randrup and P. Möller, Brownian shape motion on five-dimensional potential-energy surfaces:Nuclear fission-fragment mass distributions, Phys. Rev. Lett. **106**, 132503 (2011).

[37] J. Randrup, P. Möller, and A. J. Sierk, Fission-fragment mass distributions from strongly damped shape evolution, Phys. Rev. C **84**, 034613 (2011).

[38] L. Reichl, *A Modern Course in Statistical Physics* (John Wiley & Sons, New York, 1988).

[39] A. L. Goodman, Thermal shape fluctuations in hot rotating nuclei: Comparison of constant energy constraint and constant temperature constraint, Nucl. Phys. A **528**, 348 (1991).

[40] L. G. Moretto, Statistical description of deformation in excited nuclei and disappearance of shell effects with excitation energy, Nucl. Phys. A **182**, 641 (1972).

[41] J. Dudek, B. Herskind, W. Nazarewicz, Z. Szymanski, and T. R. Werner, Pairing, temperature, and deformed-shell effects on the properties of superdeformed ^{152}Dy nucleus, Phys. Rev. C **38**, 940 (1988).

[42] N. Schunck, J. Dudek, and B. Herskind, Nuclear hyperdeformation and the Jacobi shape transition, Phys. Rev. C **75**, 054304 (2007).

[43] J. Randrup and P. Möller, Energy dependence of fission-fragment mass distributions from strongly damped shape evolution, Phys. Rev. C **88**, 064606 (2013).

[44] K. Dietrich, J.-J. Niez, and J.-F. Berger, Microscopic transport theory of nuclear processes, Nucl. Phys. A **832**, 249 (2010).

[45] H. C. Lee and S. Das Gupta, Nuclear shape transitions at finite temperature, Phys. Rev. C **19**, 2369 (1979).

[46] A. L. Goodman, Finite-temperature HFB theory, Nucl. Phys. A **352**, 30 (1981).

[47] K. Tanabe, K. Sugawara-Tanabe, and H. J. Mang, Theory of the cranked temperature-dependent Hartree-Fock-Bogoliubov approximation and parity projected statistics, Nucl. Phys. A **357**, 20 (1981).

[48] V. Martin, J. L. Egido, and L.M. Robledo, Thermal shape fluctuation effects in the description of hot nuclei, Phys. Rev. C **68**, 034327 (2003).

[49] J. Dobaczewski, H. Flocard, and J. Treiner, Hartree-Fock-Bogolyubov description of nuclei near the neutron-drip line, Nucl. Phys. A **422**, 103 (1984).

[50] J. Dobaczewski and J. Dudek, Time-Odd components in the rotating mean field and identical bands, Acta Phys. Pol. B **27**, 45 (1996).
[51] P. Bonche, S. Levit, and D. Vautherin, Statistical properties and stability of hot nuclei, Nucl. Phys. A **436**, 265 (1985).
[52] P. Bonche, S. Levit, and D. Vautherin, Properties of highly excited nuclei, Nucl. Phys. A **427**, 278 (1984).
[53] S. Levit and Y. Alhassid, Phenomenology of shape transitions in hot nuclei, Nucl. Phys. A **413**, 439 (1984).
[54] J. Bartel, P. Quentin, M. Brack, C. Guet, and H.-B. Håkansson, Towards a better parametrisation of Skyrme-like effective forces: A critical study of the SkM force, Nucl. Phys. A **386**, 79 (1982).
[55] J. Dechargé and D. Gogny, Hartree-Fock-Bogolyubov calculations with the D1 effective interaction on spherical nuclei, Phys. Rev. C **21**, 1568 (1980).
[56] W. Younes and D. Gogny, in *The Microscopic Theory of Fission*, AIP Conf. Proc. Vol. 1175 (AIP Publishing, Melville, NY, 2009), p. 3.
[57] N. Schunck, J. Dobaczewski, J. McDonnell, W. Satuła, J. A. Sheikh, A. Staszczak, M. Stoitsov, and P. Toivanen, Solution of the Skyrme–Hartree–Fock–Bogolyubov equations in the cartesian deformed harmonic-oscillator basis. (VII) HFODD (v2.49t): A new version of the program, Comput. Phys. Commun. **183**, 166 (2012).
[58] M. V. Stoitsov, N. Schunck, M. Kortelainen, N. Michel, H. Nam, E. Olsen, J. Sarich, and S. Wild, Axially deformed solution of the Skyrme–Hartree–Fock–Bogoliubov equations using the transformed harmonic oscillator basis (II) HFBTHO v2.00d: A new version of the program, Comput. Phys. Commun. **184**, 1592 (2013).
[59] N. Schunck, Density functional theory approach to nuclear fission, Acta Phys. Pol. B **44**, 263 (2013).
[60] N. Schunck, Microscopic description of induced fission, J. Phys.: Conf. Ser. **436**, 012058 (2013).
[61] M. Baranger and M. Véneroni, An adiabatic time-dependent Hartree-Fock theory of collective motion in finite systems, Ann. Phys. **114**, 123 (1978).
[62] L. Landau and E. Lifshitz, *Statistical Physics, Part* (Pergamon Press, Oxford, UK, 1980).
[63] T. Dittrich, P. Hänggi, G.-L. Ingold, B. Kramer, G. Schön, and W. Zwerger, *Quantum Transport and Dissipation* (Wiley-VCH, Weinheim, 1998).
[64] M. Razavy, *Classical and Quantum Dissipative Systems* (Imperial College Press, London, 2005).
[65] A. V. Ignatyuk, I. N. Mikhailov, L. H. Molina, R. G. Nazmitdinov, and K. Pomorsky, The shape of the heated fast-rotating nuclei, Nucl. Phys. A **346**, 191 (1980).
[66] G. Sauer, H. Chandra, and U. Mosel, Thermal properties of nuclei, Nucl. Phys. A **264**, 221 (1976).
[67] U. Mosel, P.-G. Zint, and K. H. Passler, Self-consistent calculations for highly excited compound nuclei, Nucl. Phys. A **236**, 252 (1974).
[68] R. W. Hasse and W. Stocker, Temperature effects in the liquid drop description of nuclear fission, Phys. Lett. B **44**, 26 (1973).
[69] V. Martin and L. M. Robledo, Fission barriers at finite temperature: A theoretical description with the Gogny force, Int. J. Mod. Phys. E **18**, 861 (2009).
[70] M. Brack, J. Damgaard, A. S. Jensen, H. C. Pauli, V. M. Strutinsky, and C. Y. Wong, Funny hills: The shell-correction approach to nuclear shell effects and its applications to the fission process, Rev. Mod. Phys. **44**, 320 (1972).
[71] D. Duke, H. Carr, A. Knoll, N. Schunck, H. A. Nam, and A. Staszczak, Visualizing nuclear scission through a multifield extension of topological analysis, IEEE Trans. Visualization Comput. Graphics **18**, 2033 (2012).
[72] W. Younes and D. Gogny, Nuclear scission and quantum localization, Phys. Rev. Lett. **107**, 132501 (2011).
[73] J. Dobaczewski and P. Olbratowski, Solution of the Skyrme–Hartree–Fock–Bogolyubov equations in the cartesian deformed harmonic-oscillator basis. (IV) HFODD (v2.08i): a new version of the program, Comput. Phys. Commun. **158**, 158 (2004).
[74] D. G. Madland, Total prompt energy release in the neutron-induced fission of ^{235}U, ^{238}U, and ^{239}Pu, Nucl. Phys. A **772**, 113 (2006).
[75] H. Goutte, P. Casoli, and J.-F. Berger, Mass and kinetic energy distributions of fission fragments using the time dependent generator coordinate method, Nucl. Phys. A **734**, 217 (2004).